C U R

civieltechnisch centrum uitvoering research en regelgeving

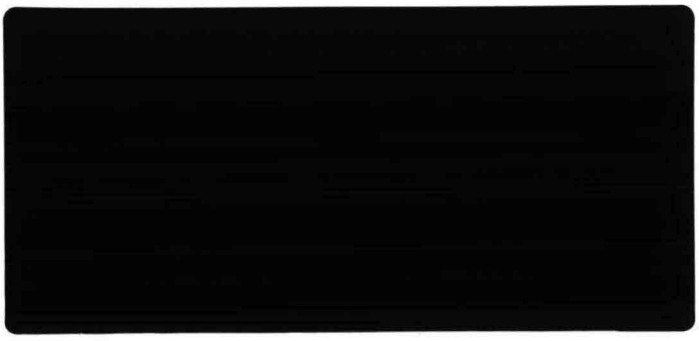

# JAMUNA BRIDGE
# BANK PROTECTION
# RESEARCH PROJECT

ANNEXE IV

Dutch prototype
experiments with bank
protection systems

1990

CUR
Postbus 420
2800 AK GOUDA
The Netherlands

# P R E F A C E

The Government of Bangladesh has set as one of its highest priorities the integration of the western and eastern regions of the country, which are presently separated by the Brahmaputra - Jamuna - Padma River system.
The Government therefore proposes to carry out a study for a multipurpose crossing, consisting of a bridge which could carry the projected traffic, a power-interconnector and a gas pipeline.
An appraisal study has been completed in 1986, (Phase I report), while the feasbility study is completed in 1988 (Phase II report).
The decision to construct the Sirajganj corridor was selected because the river banks in this corridor appear to be most stable. To guarantee stability of the bridge a number of river training works are foreseen to guide the river flow in the bridge area. High current velocities and (expected) deep scour holes make that the required training works are rather extensive and sophisticated.

For this reason the World Bank, acting as the Executing Agency for the United Nations Development Programme, has appointed the Centre for Civil Engineering Research, Codes and Specification (CUR, for short) to undertake a research project on the design of cross-sections of river training works focussed on the situation in the Jamuna Bridge area.
A Panel of Experts of the Worldbank that has been assigned to provide technical oversight of the bridge project as a whole, defined the Terms of Reference and supervised the Jamuna Bridge Bank Protection Research Project.
This project comprises a separate research project, which is complementary to the above mentioned appraisal and feasbility study.

The objective of the study is a research assignment, concerning technical advice:

a) design-principles and execution methods for bank-protection, training-dams and groynes in connection with river-training works in the direct vicinity of the upstream and downstream riverbed at the projected rivercrossing-site;
b) research on construction materials, preferably manufactured from local raw materials.

The first subject comprises mainly a review of available know-how and development of execution methods. Complementary, a laboratory test programme has been initiated, of which the results are also implemented in the report.
The research project has been prosecuted under the overall responsibility of CUR, for which CUR appointed a Supervising Committee on September 5th 1986.

After signing of the contract between the Worldbank and CUR the Supervising Committee started the project on February 15th 1988 and completed it on July 1988. The Committee has analysed the problem, formulated and sub-contracted the actual research-work in subsequent parts to the most appropriate research-institutions and consultants and reviewed the final report from the contributions of each separate part of the research sub-contracts into one comprehensive report.
The basic principle of managing and enforcement of the research project is shown below:

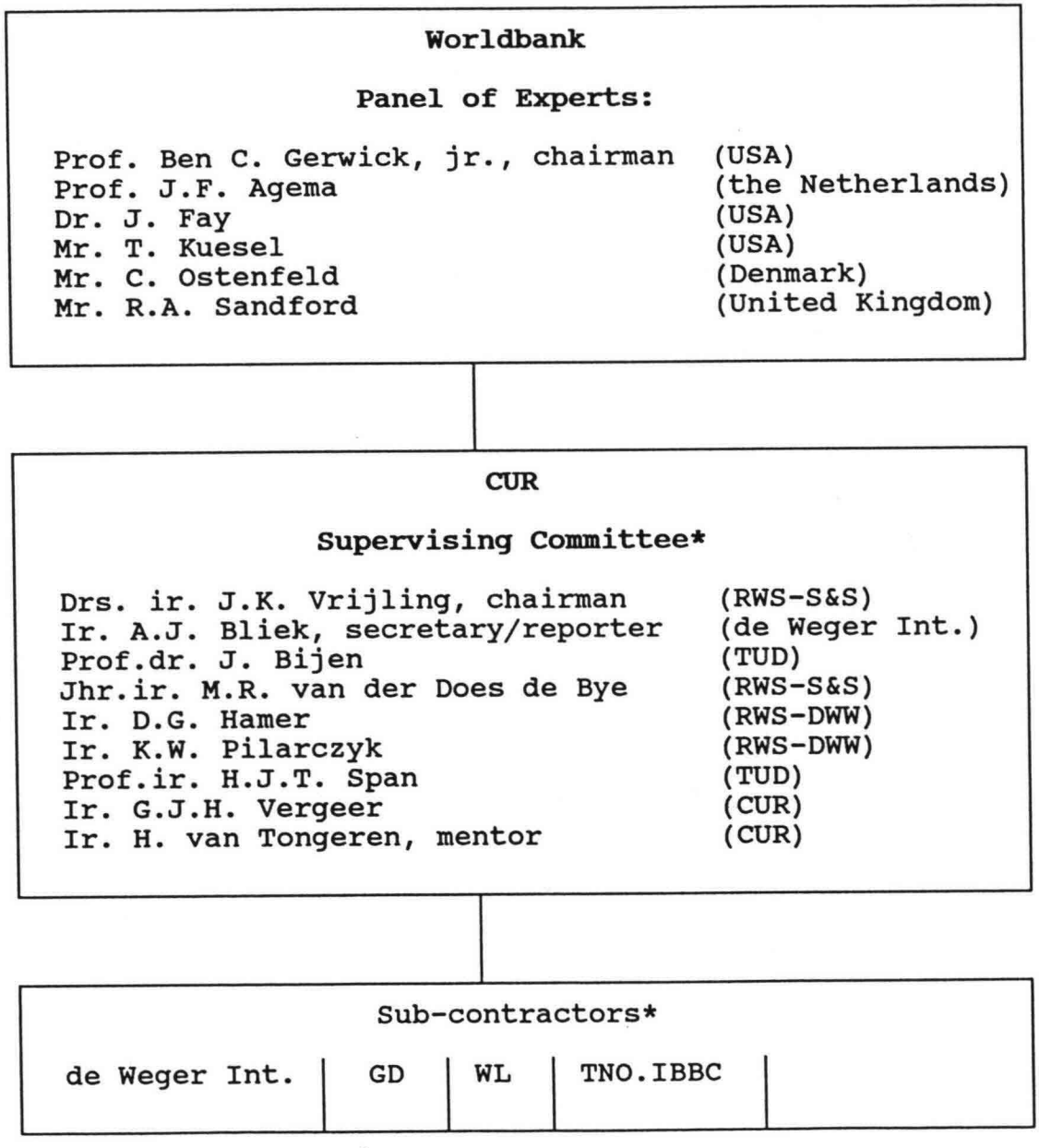

The private consulting engineering firm F.C. de Weger International has been the representative of the sub-contracted Consultant and edited the final report.
The report, including 3 annexes, has been completed in August 1988.
In this volume, annexe IV is presented separately.
In this annexe, Dutch experiments with bank protection systems in the period 1980 - 1989 are summarized.

March 1990 The Executive Committee of the CUR

* RWS-S&S = Ministry of Public Works, department of locks & weirs, Utrecht.
RWS-DWW = Ministry of Public Works, department of hydraulic engineering and research.
TUD = Delft University of Technology.
GD = Delft Geotechnics.
WL = Delft Hydraulic Laboratory.
IBBC-TNO= Institute for building materials and structures.

CONTENTS

List of figures

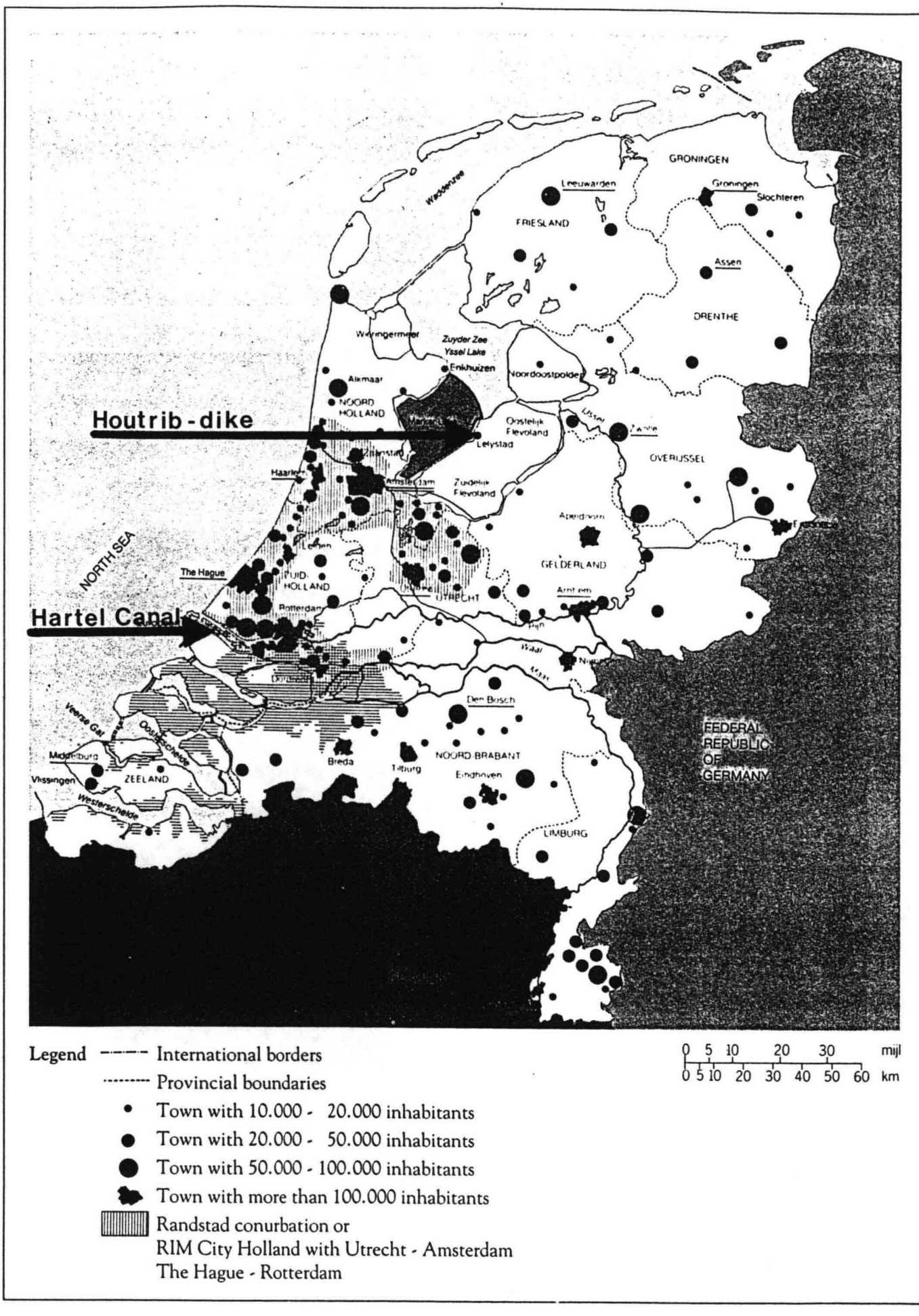


Fig. 1.1 Location of Hartel Canal and Houtrib-dike in the Netherlands

# DUTCH PROTOTYPE EXPERIMENTS WITH BANK PROTECTION SYSTEMS

## 1. INTRODUCTION

### 1.1 GENERAL

The report on the Jamuna Bridge Bank Protection Research Project (CUR, Gouda, the Netherlands, 1988), prepared on behalf of the World Bank gives a summary of the state-of-the-art design rules for bank protection systems under attack of waves or currents.
These rules are based on a longlasting experience on revetment stability worldwide and on recent research programmes, part of them still being in progress, executed in the Netherlands.

In this annexe to the afore mentioned report on the research project of the Jamuna Bridge Bank Protection two topics of these research programmes are presented:

a. the prototype experiments with numerous types of protection in the Hartel Canal close to Rotterdam

b. the prototype experiments with block mattresses at the Houtrib-dike, bordering the IJsselmeer close to Amsterdam.

It should be noted that the results of these experiments are fully included in the design rules that are given in the main report.

### 1.2 SUMMARY OF EXPERIMENTS

The location of both test sites is given in figure 1.1.

The tests in the Hartel Canal were carried out in 2 phases (1981 and 1983). The main load on the embankments of this canal is caused by the effects of ships passing through the canal, especially push barge units (up to 6 barges).
This type of load is different from normal wave attack and also different from current attack. For this reason, not only the behaviour of the embankment, but also the hydraulic loads (in function of vessel sizes, speed, etc.) were monitored in these experiments.
The results, with emphasis on the behaviour of the embankment, are dealt with in chapter 2.

The tests at the Houtrib-dike in the lake IJsselmeer were performed in 1986. The dike is open to attack by wind waves that are generated on the lake during westerly winds (fetch length some 25 km).

A number of block mats (several types) were tested here, combined with reference sections of rip-rap.
Approximately one month after completion of the test sections, the dike was subject to a severe storm that exceeded the design conditions with some 30-40% (wave height).
The results of these experiments are given in chapter 3.

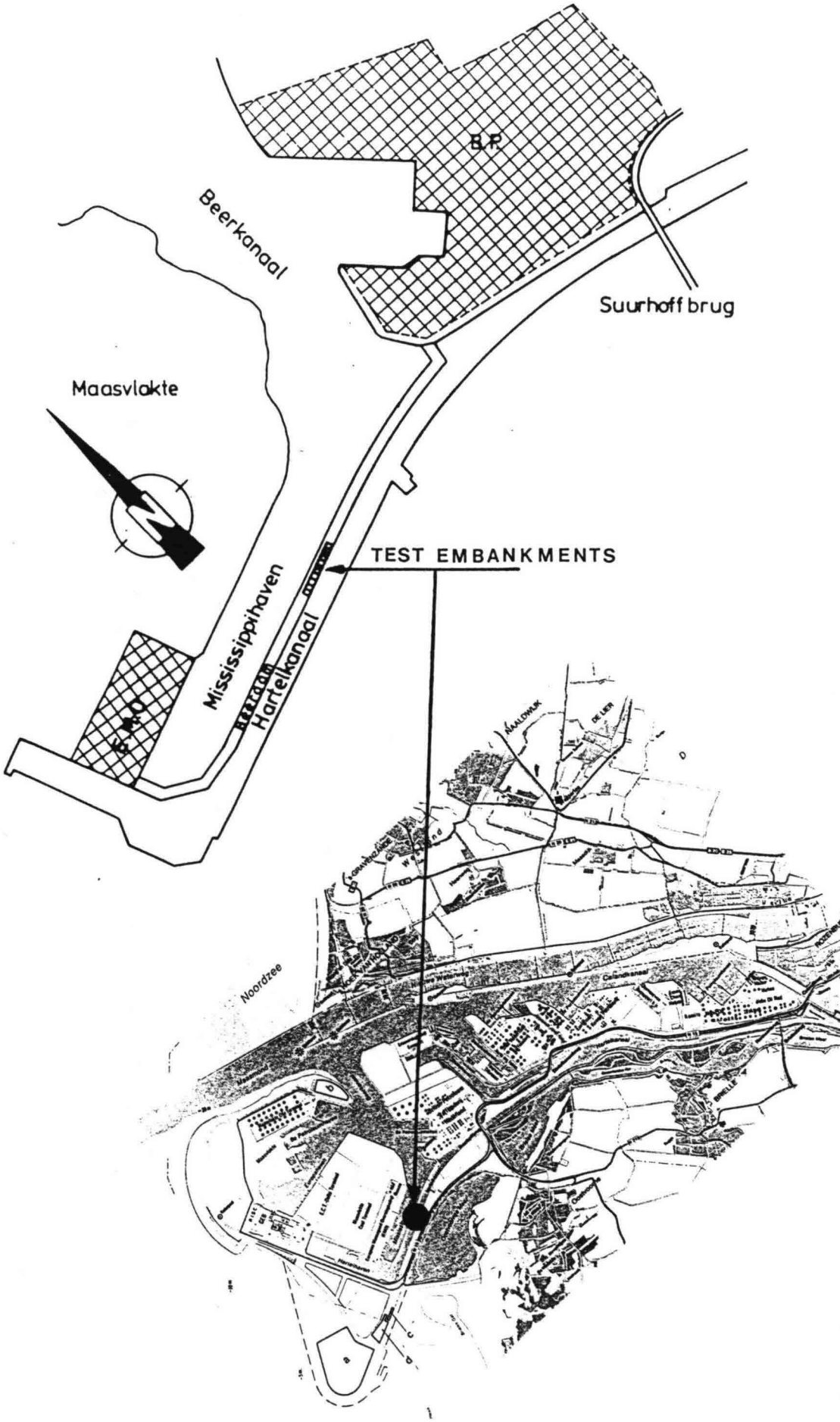


Fig. 2.1 Situation of test embankments, Hartel Canal

# 2. THE HARTEL CANAL PROTOTYPE EXPERIMENTS

## 2.1 INTRODUCTION

The prototype measurements in the Hartel Canal, a main inland navigation fairway close to Rotterdam connecting the harbour or Rotterdam/Europoort (Maasvlakte) with the river Rhine, were set up in the framework of a systematic research program on bank and dike protection.
The aim of the total research programme is to develop such design criteria that the amount of maintenance and construction costs is minimized.

Although the prototype measurements in the Hartel Canal form a part of the total programme, in this chapter that programme and its findings are only mentioned as far as it is necessary to explain the results of the prototype measurements.

The conditions of the Hartel Canal were considered to be representative for a wide range of prototype situations. The canal has a straight fairway with a restricted width (bottom width 75 m, depth 7 m), continuous slopes of homogeneous subsoil, and little disturbance by shipping. During the 1st series of measurements (1981) the Hartel Canal was closed by a navigation lock (i.e. constant water level was present). During the 2nd series (1983) the canal was in an open connection - through the tidal river Oude Maas - with the North Sea (i.e. tidal level and flow fluctuation was present).

For the first series of measurements eight different 40 m long test sections were constructed. Five others were added by different contractors in 1983.
A summary of the structure types that have been tested is given in the table on the next page.
The symbols and parameters used in this table are:

| | | |
|---|---|---|
| $D$ | = thickness of mattress or stone diameter | [m] |
| $\Delta$ | = relative density = $(\rho_s - \rho)/\rho$ | [-] |
| $\rho_s$ | = density of stone or mattress | [kg/m3] |
| $\rho$ | = density of water | [kg/m3] |

In all cases the slope of the embankments was 1 on 4 (vertical:horizontal).
A geotextile was applied under the primary armour in those cases where a relatively open structure was placed directly on a fine sublayer.
In appendix 1 an illustration is given of all slope protection systems that have been installed in the Hartel Canal.

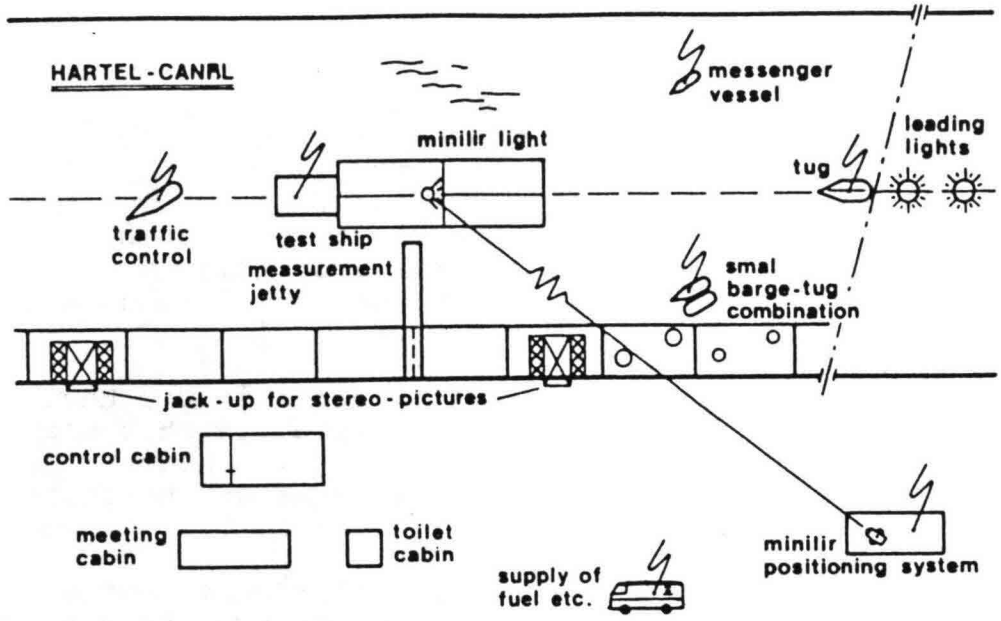


a. Lay-out of monitoring system

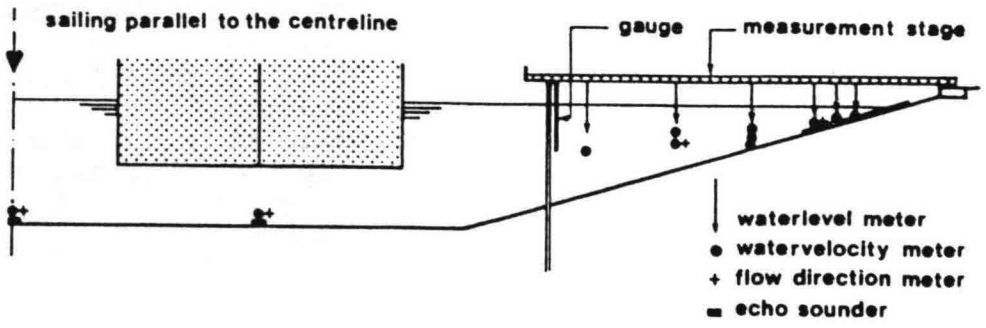


b. Cross section at central measurement stage

Fig. 2.2 Schematized set-up of prototype measurements

| embankment type | thickness D toplayer | relative density Δ | ΔD |
|---|---|---|---|
| **loose materials** | | | |
| . fine gravel (30-80 mm) on sand | ~0.045 m | 1.6 | 0.07 |
| . coarse gravel (80-200 mm) on sand | ~0.14 m | 1.6 | 0.22 |
| . rip-rap (5-40 kg) on sand | ~0.20 m | 1.6 | 0.32 |
| . ditto on clay | ~0.20 m | 1.6 | 0.32 |
| **block pitching** | | | |
| . blocks 0.15 m thick on clay | 0.15 m | 1.35 | 0.20 |
| . ditto on sand | 0.15 m | 1.35 | 0.20 |
| . ditto on gravel | 0.15 m | 1.35 | 0.20 |
| **interlocked block revetments** | | | |
| . basalton on sand | 0.15 m | 1.35 | 0.20 |
| . ditto on silex | 0.12 m | 1.35 | 0.16 |
| . Armorflex mats | 0.11 m | 1.35 | 0.15 |
| . ACZ-Delta mats | 0.16 m | 1.35 | 0.22 |
| **miscellaneous** | | | |
| . sand-sausage mattress Profix | 0.20 m | 1.0 | 0.20 |
| . PVC-Reno mattresses (gabions) | 0.17 m | 1.0 | 0.17 |
| . Fixtone open stone asphalt | 0.15 m | 1.0 | 0.15 |

## 2.2 SITUATION

The situation of the test sections along the border of the Hartel Canal is given in figure 2.1. In figure 2.2 the measuring instruments that were installed are shown.
The typical cross-section of the test sections is given in figure 2.3.
The loads on the embankments were generated by sailing vessels, mainly pushing units.
The test embankments (top-layer and subsoil), test-ships and wet cross-section of the test location were equipped with various instruments. The measurements were centrally directed from a shore-based "central" cabin (see figure 2.2). Just before entering the test-section of the canal by a test-ship, all instruments started operating simultaneously on a command given in the central cabin. Processing of the data followed immediately, resulting in plots of the selected signals. By analyzing the plotted information in conjunction with erosion measurements, a well balanced selection of the next required test conditions could be made.

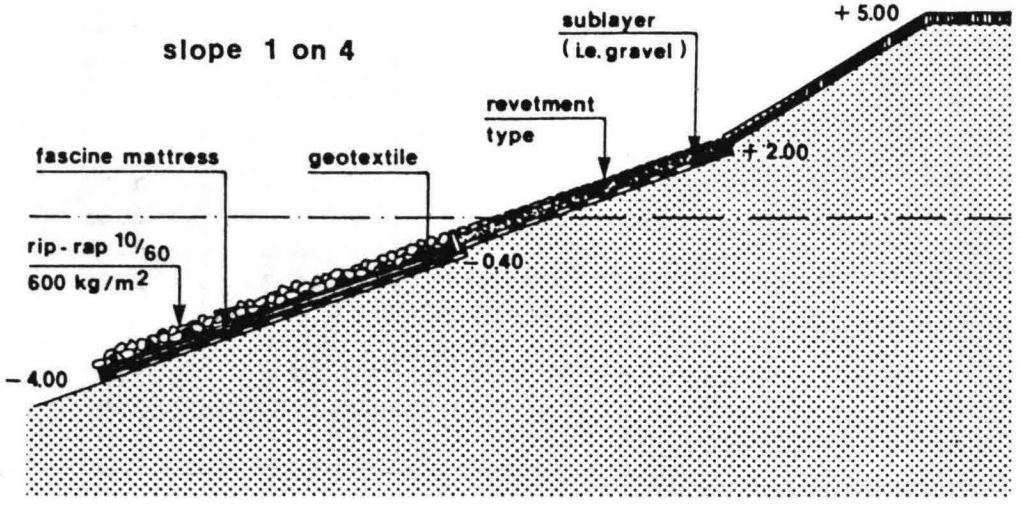


Fig. 2.3 Typical cross section of prototype embankments

## 2.3 INSTALLED INSTRUMENTS

a. Hydro instruments. To obtain a thorough insight into ship induced water motion, detailed measurements of wave heights, velocities and turbulence were carried out. Wave height meters, flow velocity meters and flow direction indicators were fixed to the measurement jetty (see figure 2.2). A wave run up device was installed on the slope. Moreover, some other hydro measurements were carried out, viz.: measurements of pressures along the slope, measurements of vertical flow distribution (to determine development of the boundary layer), measurement of turbulence rate in the immediate vicinity of the rip-rap, and measurement of rate and direction of velocity, pressure and vertical distance to the ship (by means of echosounder) in the line of the ship path.

b. Soil mechanical instruments. A number of water pressure gauges were placed into the subsoil before the filter cloth and top layers were put into place. These gauges were situated in such a manner that both horizontal and vertical gradients were measured. Beforehand, 6 concrete blocks and 3 basalton blocks had also been provided with pressure gauges on both sides of the blocks which made it possible to determine the absolute pressure and the pressure difference exerted on the protection blocks when attacked by ship induced waves. All hydro-, and soil mechanical instruments were directly connected to the central data acquisition system.

c. Erosion control. A number of preparations and devices were applied to determine the beginning of motion and/or erosion of protective materials. These were: coloured sections of gravel and rip rap, flat cylindrical gravel traps (to catch the gravel) and a jack-up for stereo pictures at rip-rap locations. When the ship had passed divers immediately inspected the embankments under the waterline, collected eroded rip-rap and surveyed the four gravel traps. All trapped material was carefully analysed. From time to time the erosion holes were filled with the aid of a barge-tug combination.

d. Instruments aboard of test ships. On board of the test ships the following parameters were recorded: course and rudder-angle, trim of the barges, and torque and number of revolutions of the shafts. A gyrocompass was used to determine the course. All signals were recorded as a function of time. Transfer to a function of place is only possible when a very accurate position system is used. Data recorded on board during a run were directly collected by a liaison boat and taken to the central cabin.

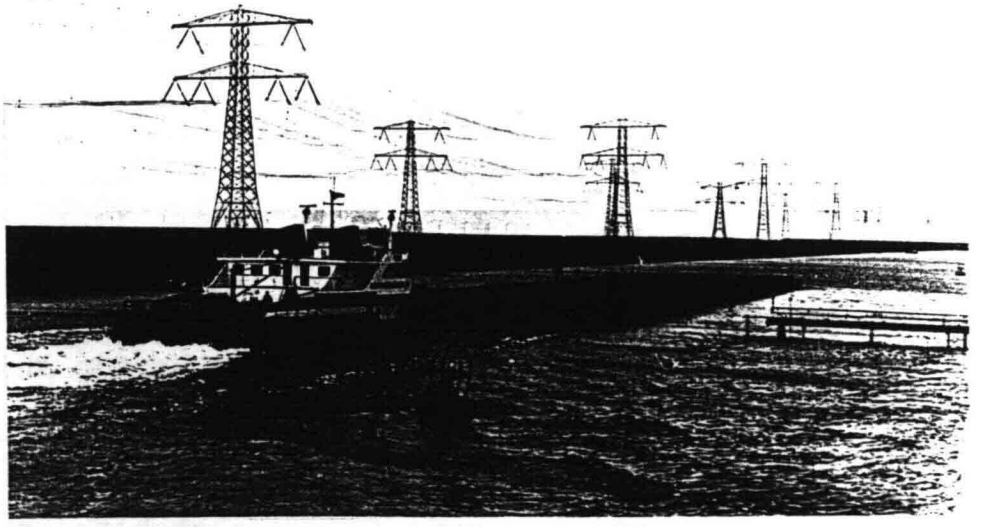

Fig. 2.4 Pushing unit 2 x 3 loaded
length 153 m, width 35.4 m, draught 3.0 m
sailing along the test site

Fig. 2.5 Pushing unit 3 x 2 loaded
length 229.5 m, width 23.6 m, draught 3.0 m

e. Positioning system. In the prolongation of the Hartel Canal leading lights were placed to show which course the test ships had to maintain (centerline or toe of slope). The exact position of the test ship was determined with a Minilir system in conjunction with an automatically operating distance meter (Aga-120). Through the continuous registration of these instruments the ship's position was accurately determined. Both the position of the ship in the fairway and the total sinkage and trim of the barges were stored and added to the central acquisition system immediately after each test run.

## 2.4 HYDRAULIC LOADS

During the 1st series of measurements (1981) the following test ships were used:
- small vessel for management
- pushing unit, 4500 hp, with barges (length each barge 76.5 m, width 11.8 m and draught 3.0 m); four loaded barges in 2 x 2 formation, four empty barges and six loaded barges in 3 x 2 and 2 x 3 formation (see figures 2.4 and 2.5)
- tug, 700 hp.

During the 2nd series of measurements (1983) the following test ships were used:
- pushing unit; 5400 hp, four loaded barges in 2 x 2 formation (one test run was also done with four empty barges)
- motor vessel, 800 hp (80 m x 9.5 m x 2.5 m)
- tug, 1120 hp.

The number of test runs with each test ship and the maximum values of watermotion components induced by test ships are summarized on the next page.

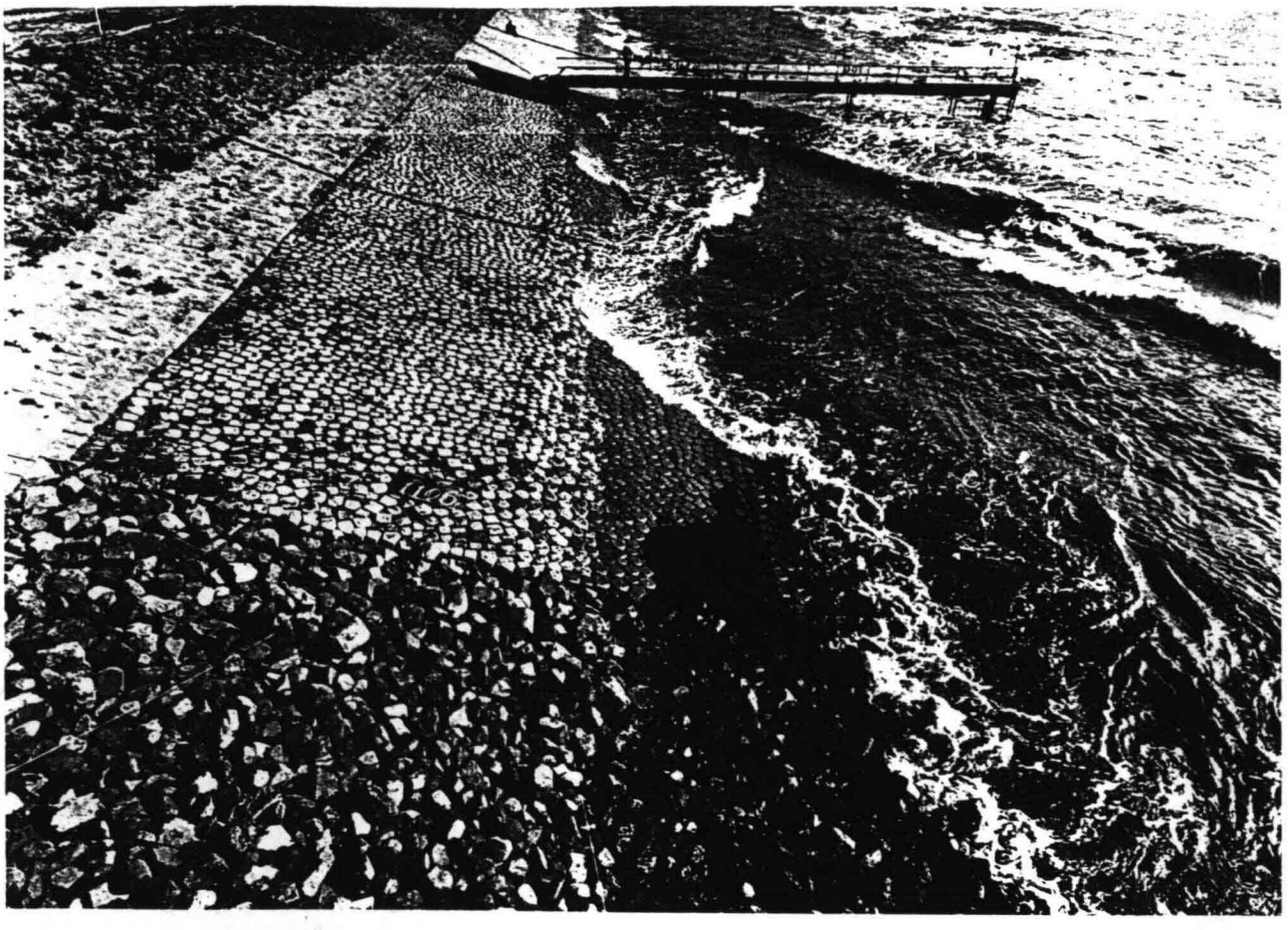

Fig. 2.6 Ship induced wave attack on the test embankments

| Test ship | Position | no. of turns | $V_R$ (m/s) | Z (m) | H (m) |
|---|---|---|---|---|---|
| 1981 | | | | | |
| push barges: | | | | | |
| 2 x 2, loaded | centerline | 19 | 1.27 | 0.75 | 0.40 |
| 2 x 2, loaded | toe of slope | 21 | 2.02 | 0.85 | 0.40 |
| 2 x 2, empty | toe of slope | 7 | 0.85 | 0.73 | 0.86 |
| 2 x 3, loaded | toe of slope | 4 | 1.52 | 0.84 | 0.21 |
| 2 x 3, loaded | centerline | 4 | 1.35 | 0.67 | 0.20 |
| 3 x 2, loaded | toe of slope | 3 | 1.12 | 0.56 | 0.30 |
| 3 x 2, loaded | centerline | 6 | 1.06 | 0.45 | 0.27 |
| tug | toe of slope | 2 | | | |
| 1983 | | | | | |
| push barges | | | | | |
| 2 x 2, loaded | toe of slope | 34 | 1.85 | 1.15 | 0.35 |
| 2 x 2, empty | toe of slope | 1 | 0.75 | 0.55 | 0.75 |
| motor-vessel | toe of slope | 16 | 0.60 | 0.35 | 0.30 |
| tug | | 38 | - | - | 0.80 |

$V_R$ = velocity of return flow, Z = max. waterlevel depression, H = height of secondary waves.

The magnitude of these parameters have been actually observed in the Hartel Canal during the tests.
An example of the ship induced wave attack on the embankments is given in figure 2.6.
Theoretical and practical considerations and relationships to determine these parameters from the ship characteristics are given in appendix 2, attached to this report. In this appendix use is made, among others, of the results of the prototype measurements discussed here.

## 2.5 BEHAVIOUR OF TEST EMBANKMENTS

Figure 2.7 shows the main characteristics of a number of the protection systems that have been installed.

### 2.5.1 Loose materials

a. Gravel on geotextile and sandy subsoil. Two gravel embankments, one with 30 - 80 mm gravel (fine) and the other with 80 - 200 mm gravel (coarse), were applied to verify the model relations describing the beginning of movement and transport of loose materials under ship induced water motion. High gravel transports were only observed when push tows and tugs sailed at high speed near the bank. In general, calculation methods based on model results give a proper approximation of the prototype values.

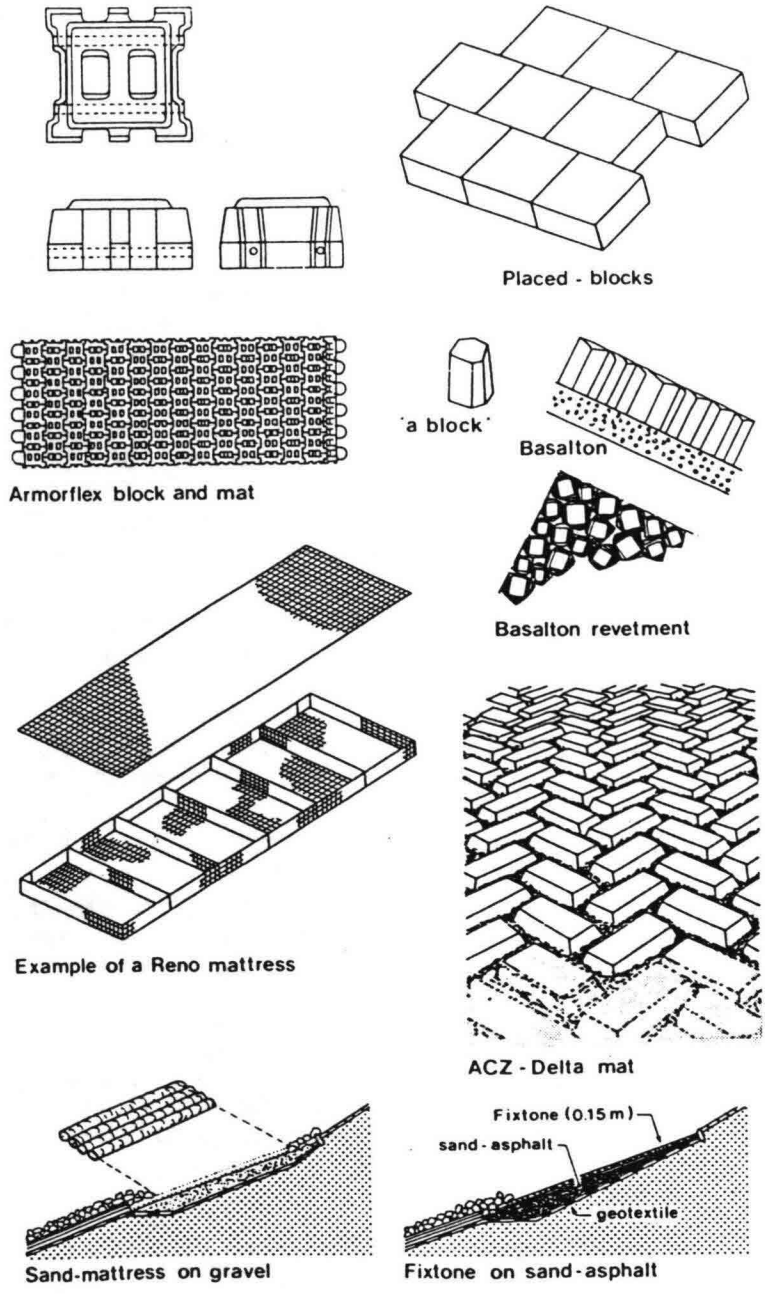


Fig. 2.7 Examples of systems tested in the Hartel Canal

It is interesting to note, that during the period between the two series of prototype measurements (October 1981 - May 1983) an unexpectedly high transport of fine gravel took place as a result of a normal (rather low) shipping intensity in the Hartel Canal. The probable explanation could be, that more vessels (particularly small vessels and tugboats) are sailing nearer to the bank than expected at the first sight. It also emphasizes the necessity of sufficient statistical data on behaviour of ships in navigation channels to be able to properly predict a longterm transport balance.

b. Rip-rap 5-40 kg on geotextile. For this class of rip-rap beginning of movement was rather exceptional. It has been observed to occur mainly due to secondary waves induced by empty barges and tugs sailing very close to the bank (i.e. at the toe of the slope). The two types of subsoil that were considered (sand and clay respectively) did not result in any significant differences in behaviour of the rip-rap slope protection. It can be concluded that in the most practical cases this, or a little higher class of rip-rap would be satisfactory for normal inland fairways. In the Netherlands the stone classes used normally for bank protection of channels with high shipping intensity (incl. push-tow) are of the 10-60 kg and/or 60-300 kg types.

### 2.5.2 Placed (free) blocks

In the Netherlands, concrete blocks are frequently used for the revetments of dikes, dams and banks. In general, no reliable design criteria are as yet available for these (and also for interlocked) revetments. In all these cases, the type of sublayer (permeable/impermeable) and the rate of permeability of the blocks are very important factors for the stability of these revetments. Sometimes, these blocks are threaded with cables or connected to a geotextile by nails or nylon nooses (or even glued) forming a flexible and structurally integrated mat system.

For the prototype tests, 0.3 m x 0.2 m and 0.15 m thick concrete blocks were used. Both sand and clay were used to form a subsoil. No failure of the revetment has been observed (e.g. no uplifting of blocks). However, limited settlements and thus deformation of the revetment has been observed at various places where the underlayer consisted of sand and geotextile.
Analysis of the registration of the pressure gauges below the blocks has indicated that the hydraulic gradients at the intersurface of sandy subsoil and geotextile often exceeded the critical values for the beginning of erosion.

Because of the geotextile the vertical transport was limited and the main transport took place probably along the slope. Some amount of sand could get lost due to a lack of adequate sand tightness at the transition from the block revetment to the rip-rap toe protection.

### 2.5.3 Flexible interlocked block revetments

Three types of flexible interlocked revetments with three different principles of interlocking were used for the prototype tests, namely: basalton blocks, Armorflex mats and Delta block mats (ACZ).

a) Basalton blocks (prisms). The excellent experience the Netherlands has had with natural basalt revetments (stone pitching) in conjunction with its increasing costs because of the shortage of natural basalt, have resulted in the development of artificial concrete prisms based on the shape of the natural basalt (patented as "Basalton"). This system is characterized by a polygon connection and consists of various shapes and different dimensions of prisms which allow even the construction of a random shaped revetment. The blocks are produced in various sizes and with various densities. Lately they are also available as Basalton mats. The area of the interblock space equals about 20% of the total surface area. The blocks are slightly tapered vertically. Because of this, the prisms may sink lower if there is any settlement of the soil-body or erosion of the sublayer, which is immediately evident for this reason. Moreover, because of its tapered shape, the prisms have a firm position in the slope. The interstices between the blocks are filled with, for instance, graded broken stone, silex or copper-slag (size 1-50 mm). As a result, the possibility of upward movement of the blocks is strongly reduced. In the Netherlands, the underlayer normally consists of graded broken stone of silex stone (a waste product of the cement industry) of 0-60 mm and about 0.3 m thick (i.e. for sea-dikes).
It is also possible to place Basalton blocks on sand-soil with a geotextile and broken stone in between. Recently full scale tests on this type of revetment were performed in the large Delta Flume of the Delft Hydraulics Laboratory. As a result of the filling of the interstices with granular material the strength of the structure may increase to very high levels. These high values are not recommended for practical applications however, because of the fact that the ideal circumstances of the laboratory test sections will never be present in reality over the whole revetment length and over the whole lifetime of the structure. Moreover, the stability of the filter and the subsoil may become critical in this case.

The behaviour of the Basalton revetment, used in the prototype tests in the Hartel Canal, was very satisfactory. During the first series of measurements (1981) only 0.15 m thick blocks were used. During the 2nd series (1983) 0.12 m high blocks were also applied. In both cases no stability problems occurred. The washing out of the granular material was, on average, restricted to a few centimetres in depth.
This aspect leads to the restriction that the thickness of the blocks should never be less than approximately 0.10 m, even under very moderate wave attack.

b) Armorflex block mats. The purpose shaped interlocking Armorflex blocks are threaded with steel or nylon cables and bounded together, thus forming a flexible mat system. A geotextile and/or a graded filter are firstly spread over the slope to be protected, and than overlaid by the block mat. Additionally, granular material may be applied to the interblock spaces to rigidify the mat once it is in place. Because of the cabling, this system maintains its integrity in the event of subgrade deformation or severe dynamic loading up to a certain exceedance of the design conditions for free blocks. The Armorflex mat system has been investigated extensively with respect to wave attack.

   For the prototype test embankments in the Hartel Canal both full and cellular type blocks of 0.11 m height were used. The interstices of both systems were filled with fine gravel. The performance of these systems was very satisfactory. Against expectation the washing out of the grouting material was rather limited.

c) ACZ Delta block mats. The system is characterized by a diagonal block distribution and consists of rectangular purpose shaped blocks (blocks 0.20 m x 0.40 m underneath and 0.155 m x 0.355 m upper surface). The blocks are poured onto the geotextile. The connection between blocks and geotextile is realized by four nylon nooses connected to the geotextile.
   The space between the blocks in the test section was about four centimetres wide. The block mats (block height 0.16 m) were placed on gravel; interstices were also filled with gravel.
   However, due to the fact that the ratio between the interstices and the nominal diameter of the applied gravel was rather large, the fill material was soon washed out and the external hydraulic load was acting through the geotextile directly on the sand sublayer. In the long run this may lead to erosion of the sublayer and deformation of the revetment, if the mat is directly placed on a sand sublayer instead of on a gravel layer as was done in the Hartel Canal. The short term performance of this mat did not lead to instability problems.

Even after 4 years of exposure to the ship induced wave action in the canal, only minor settlements were observed in the Hartel canal tests.
In general, the weak point of all types of block mats is how to repair them when the sublayer erodes and/or when the (under-water) connection of adjoining mats fails.

### 2.5.4 Sand-sausage mattresses (Profix).

Zinkon B.V., a Dutch company specialized in bank and slope protection works, has developed a flexible erosion control system composed of filter-cloths and granular fill material, known as the Profix system. Profix is a fast and relatively cheap method. Two tightly woven polypropylene cloths are stitched together at regular intervals to give a design weight of at least 200 kg/m2 when filled with sand. Both filter cloths must be sand tight. Moreover the outer cloth is stabilized against ultra violet radiation. It is provided with a felt layer to promote and develop vegetation that provides extra protection against u.v. radiation. The cloths allow plant roots to penetrate into the subsoil thus providing extra stability to the construction. The required strength of the filter cloths depends on the exerted loads, the design of the slopes, the method of construction, the thickness and the weight of the fill material. Sand and/or gravel are very suitable as fill material, possibly mixed with cohesive additives. Mixing the fill with seeds can promote vegetation. The empty mattress is spread out at the top of the revetment and pulled out in stages, as they are filled, into the river or channel. Dry sand is blown through rubber hoses threaded in turn into flap covered openings every 5 to 10 m along each tube of the mattresses.
These mattresses are actually used on a large scale for bank protection works in the Nigerian Delta area (since 1981).
Special attention has to be paid to the risk of vandalism i.e. the mats may be cut away on purpose or damaged by pins through them. However, this has not been experienced. For areas which are not so densely populated (i.e. no serious risk of vandalism) this system may offer a good alternative bank protection.

The Profix mattress at the test embankment had an average thickness of 0.20 m containing medium to coarse sand, between a flat laying filter cloth sticked together at intervals of 0.40 m. The direction of the tubes was up and down the slope.
The experience with this system obtained through the tests in the Hartel Canal showed the high importance of a sufficient degree of density (compaction) of the sand inside the mattress.

Due to breakdowns of the filling equipment this degree, unfortunately, was not obtained and migration of sand grains inside the tubes downward the slope could take place. This as a result of the water movements caused by tidal action and passing ships.
Consequently, the part of the mattress below the maximum water level was densified affecting the filling degree of the upper part. After refilling this part of the mattress the performance of the construction appeared to remain more satisfactory.

2.5.5 PVC Reno mattresses (Maccaferri Gabions).

A gabion is a large wire mesh basked coated with zinc or PVC (polyvinyl chloride) to ensure long life under adverse conditions. It is rectangular in shape, variable in size with diaphragms at certain intervals. These baskets, filled with relatively small rock, are widely used in bank stabilisation and river training structures. The inherent flexibility of the gabions - the ability to bend without breaking - seems to be the primary reason for their success. Other important advantages are its permeability, stability, easy repair and relative economy.

The mattresses used in the prototype tests were PVC coated baskets 1.0 m x 4.0 m and 0.17 m thick, filled with coarse gravel 70 - 130 mm and placed on a geotextile on sand. The performance was satisfactory. However, the placement was done with more than normal care. After the tests only a slight swelling of the individual cells was observed. Also, only a limited number of stones has escaped throughout the wire mesh of the mattress baskets. The gabions show to be a good alternative for locations where vandalism is not a problem.

2.5.6 Fixtone (Bitumarin B.V.)

Fixtone (open stone asphalt) is applied since 1968 as a modern development in the construction of permeable asphalt revetments. Fixtone is produced in a asphalt mixing plant in two phases. In the first phase a sandmastic is produced with a composition: 62% sand, 20% filler and 18% straight run bitumen. The composition can vary due to differences in raw materials to be applied. In the second phase this sandmastic is mixed with crushed lime stone (20/40 mm or 16/22 mm) in the ratio: 82% stone and 18% sandmastic. The two phases are succesively carried out in one mixing procedure. The Fixtone has a void ratio of approx. 25% with pores having a diameter up to 10 mm.
The Fixtone revetment generally consists of a layer of fixtone on a filterlayer. This filterlayer may consist of a layer of lean sandasphalt or a filterfabric to prevent subbase material to wash out.

For slope and bottom protection under water Fixtone can be applied as a prefabricated mattress including a sand-tight filterfabric.
Due to the complicated visco-elastic properties of asphalt mixes, which cannot be scaled down, the assessment of resistance to wave attack can only be carried out on actual scale. In order to provide a design tool for designers, the experience from several projects in combination with the application of the theoretical models has been compiled into a "rule of thumb", reading:

$$D = C.H_s$$

in which D = thickness of the Fixtone layer, $H_s$ = significant wave height and C = coefficient, being 1/6 in the case of Fixtone on a filtercloth and 1/10 on a sandasphalt filter. This rule is also supported by large scale check tests in the Delta flume of the Delft Hydraulic Laboratory. By taking a relative density $\Delta$ of the Fixtone of 1.0, this leads to a $H_s/\Delta$ D-value of 6-10. Large scale tests in the Delta flume show figures up to 13. Siltation or growth of algaes in the relatively small pores of the Fixtone may reduce these very high stability figures.

The prototype test embankment in the Hartel Canal consisted of a 0.15 m thick toplayer of Fixtone (stone size 20/40 mm) on an average 0.15 m thick layer of lean sandasphalt. The shortterm performance of Fixtone was rather satisfactory. As the surface was not finished by slight compaction, a very small number of stones loosened as was expected due to wave attack.

In general the conclusions and experiences correspond with the conclusions of large scale tests in the Delta Flume where wind waves up to $H_{max}$ = 2.65 m were generated on a similar structure. Longterm abrasion tests are being carried out in the large stream flume at Lith in the Netherlands. The results indicated an acceptable durability of the surface under longterm loadings (3 weeks) of an intermediate dynamic loading by a waterjet generated from a hydraulic head of 4,0 m. Currents up to 6,0 m/sec and more were generated on the surface.
For details with respect to the design and execution methods of Fixstone reference is made to annexe II to the main report.

## 2.6 STABILITY CALCULATIONS

The standard parameter for the determination of the stability of primary armour layers of a slope under attack of waves reads:

$$H_s / \Delta D$$

where:

| | | |
|---|---|---|
| $H_s$ | = significant wave height | [m] |
| $\Delta$ | = relative density $(\rho_s - \rho)/\rho$ | [-] |
| $\rho_s$ | = density of primary armour | [kg/m3] |
| $\rho$ | = water density | [kg/m3] |
| D | = thickness of primary armour layer or stone diameter | [m] |

In section 2.1 all types of slope protection that have been applied are specified in terms of their $\Delta$D-value.
A rough estimate of the loads on the structures can be obtained by taking the height of the secondary wave as given in section 2.4, being in 1981 0.86 m at maximum (average of 7 turns), and in 1983 0.80 m at maximum (average of 38 turns) and by assuming that this wave can be considered to be a significant wind wave.

From appendix 2 can be seen that this approach is not completely correct, as ship induced loads cannot be set equal to wind wave attack.
Nevertheless, this approach is giving an idea on the stability factor, i.e. the ratio between load and strength.

The strength of the structure is expressed in a maximum acceptable value of $H_s/\Delta D$. This maximum depends on:
- the structure type ($\phi$-coefficient)
- the slope angle $\alpha$
- the wave breaking parameter $\xi_z$, defined as:

$$\xi_z = \tan \alpha / \sqrt{H_s/L_o}$$

where:

| | | |
|---|---|---|
| $L_o$ | = $g.T_z^2 / 2\pi$ | [m] |
| g | = acceleration due to gravity | [m/s2] |
| $T_z$ | = average wave period | [s] |

The effect of $\xi_z$ and $\alpha$ on the strength of the structure is also a function of the type of structure. For details reference is made to the main report.
To simplify the presentation, the effects of $\xi_z$ and $\alpha$ are not presented separately here; they are included in the value of $\phi$.

The table presented on the following page shows for each system:
- its $\Delta D$-value
- its load ($H_s$-value)
- its $H_s/\Delta D$ value
- its $\phi$-value
- its stability factor f, being the ratio between $\phi$ and the actual $H_s/\Delta D$.

| protection type | $\Delta D$ [m] | $H_s$ [m] | $H_s/\Delta D$ [-] | $\phi$ *) [-] | f [-] | stability indication |
|---|---|---|---|---|---|---|
| fine gravel | 0.07 | 0.86 | 12.3 | 2.25 | 0.18 | failed |
| coarse gravel | 0.22 | 0.86 | 3.9 | 2.25 | 0.58 | failed |
| rip-rap | 0.32 | 0.86 | 2.7 | 2.25 | 0.83 | failed |
| pitched blocks | 0.20 | 0.86 | 4.3 | 3.0 | 0.70 | failed |
| basalton 0.15 m | 0.20 | 0.86 | 4.3 | 4.0-6.0**) | 0.93-1.40 | stable |
| basalton 0.12 m | 0.16 | 0.80 | 5.0 | 4.0-6.0**) | 0.80-1.20 | stable |
| Armorflex | 0.15 | 0.80 | 5.3 | 4.0-6.0**) | 0.75-1.13 | stable |
| ACZ-Delta | 0.22 | 0.80 | 3.6 | 4.0-6.0**) | 1.11-1.67 | stable |
| Profix | 0.20 | 0.80 | 4.0 | 3.5 | 0.88 | failed |
| PVC-Reno | 0.17 | 0.80 | 4.7 | 4.5 | 0.96 | failed |
| Fixtone ("young") | 0.15 | 0.80 | 5.3 | >6.0 | >1.13 | stable |

*) $\phi$ includes the effects of the slope angle (1 on 4) and a wave breaking parameter $\xi_z = 1$
**) the higher values refer to a situation with gravel filled interstices.

From the table can be concluded that the loads on 6 bank protection systems exceeded the design criteria (stability factor lower than 1).
Nevertheless, only for the gravel and the rip-rap displacements were observed (the rip-rap being "rather exceptional beginning of movement" only).
This may indicate that design criteria ($\phi$-values) for some of the bank protection systems are on the safe side.
On the other hand, the simplifications applied (ship induced wave is comparable to significant wind wave) are not correct, both with respect to the water motion and with respect to the duration of the attack (a few waves or a whole storm).
Final conclusions cannot be drawn for this reason.

## 2.7 CONCLUSIONS

The behaviour of the test embankments in the Hartel Canal was in general satisfactory.
Only on the gravel revetments significant displacements could be observed (as expected).
According to the calculations presented in the previous section, 4 other types had a stability factor lower than 1 (failure), i.e.:
- rip-rap
- pitched blocks
- Profix sand-sausage mattress
- PVC-Reno gabions.

In reality, only the rip-rap was subject to "rather exceptional beginning of movement"; the other systems were stable.
Two reasons can be given for this discrepance:
a) the assumptions made in the determination of the hydraulic loads
b) may be the stability criteria are on the safe side.

The other 5 systems that have been tested were stable, both in nature and according to the calculations.

Additional remarks can be made about 2 systems:
ACZ-Delta block mats. Due to the fact that the ratio between the interstices and the nominal diameter of the applied gravel was rather large, the grouting material was soon washed out and the external hydraulic load was acting through the geotextile directly on the sublayer. In the long run this may lead to erosion of the sublayer and deformation of the revetment (not observed in the Hartel Canal). Improvement of the system i.e. reducing the space between the blocks, has in the meantime been accomplished.
Sand sausage mattresses (ProFix). Due to breakdowns of the filling equipment the required degree of density (compaction) was not obtained and migration of sand grains inside the tubes downward the slope could take place. After refilling this part of the mattress the performance of the construction appeared to remain more satisfactory.

From the extensive measurements on the hydraulic conditions that have been carried out during the tests and the observed erosion of the gravel sections stability criteria could be determined for ship induced wave attack.
These criteria refer to the velocity of the return flow, the waterlevel depression in front of the transverse sternwave and the secondary waves that are generated by passing vessels.
A summary of these design criteria is also given in appendix 2, attached to this report.

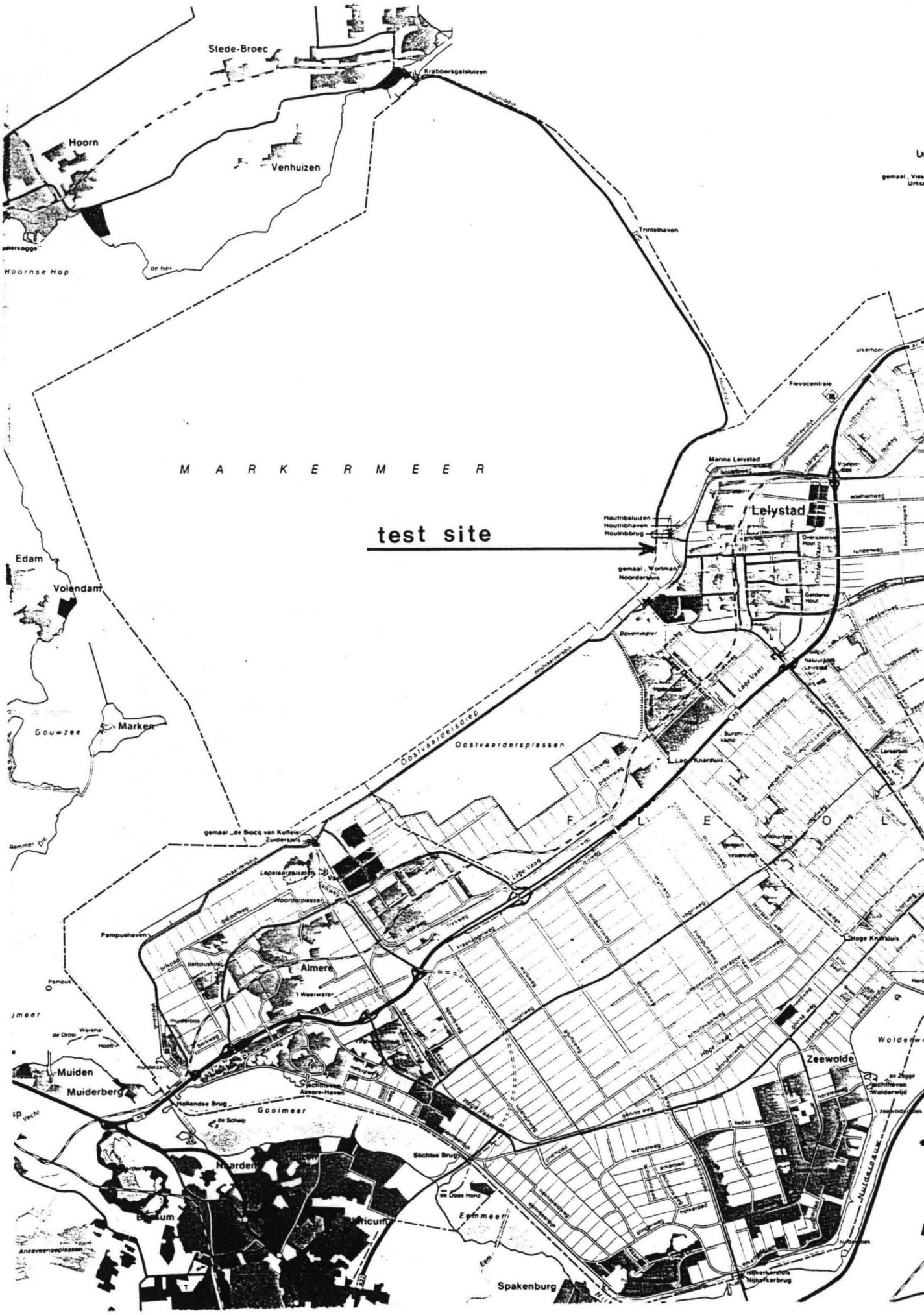


Fig. 3.1 Location of Houtrib-dike test site in the lake Markermeer/IJsselmeer

# 3. EMBANKMENTS IJSSELMEER (HOUTRIB-DIKE)

## 3.1 INTRODUCTION

The prototype tests on block mats along the dike in the IJsselmeer between Enkhuizen and Lelystad (Houtrib-dike) were carried out in view of future development plans in that area.
In these plans the construction of a number of dikes is foreseen. These dikes have to be constructed on a subsoil that is subject to significant settlements that may vary from place to place.

When compared to the traditional solution, consisting of rip-rap on a filter structure, block mats have the adventage that they are flexible.
Differences in settlement behaviour of the subsoil can be met very simply using block mats.
Moreover, recreational use of the embankment is more attractive when block mats are applied.

As there are numerous types of block mats on the market, it was decided to apply four types in the tests, each of them to be supplied by different manufacturers.

The dimensions of each of these types were determined in such a way that it would be likely that the actual wave attack would come close to the design conditions in a period of 2-3 years.
The test sections were installed in September 1986; final conclusions were drawn in 1988/89.

## 3.2 SITUATION

The location of the test sections is given in figure 3.1. They are prone to wave attack from westerly directions, the fetch length being some 25 km.

The lake normally has a more or less stagnant waterlevel. During storms from westerly directions wind and wave set up may occur.

Currents can be neglected.

The waterdepth at the toe of the dike amounts some 4 metres.

The length of the test sections varied between 30 and 40 metres, while both at the nothern and the southern end a section of rip-rap (natural stone) of 25 m was added for reference purposes. See figure 3.2.

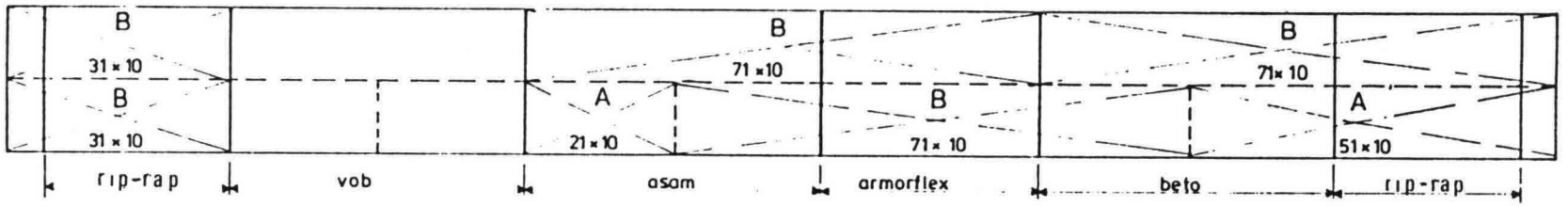


A= nicolon 66573

B= nicolon 66373

## SITUATION GEOTEXTILES

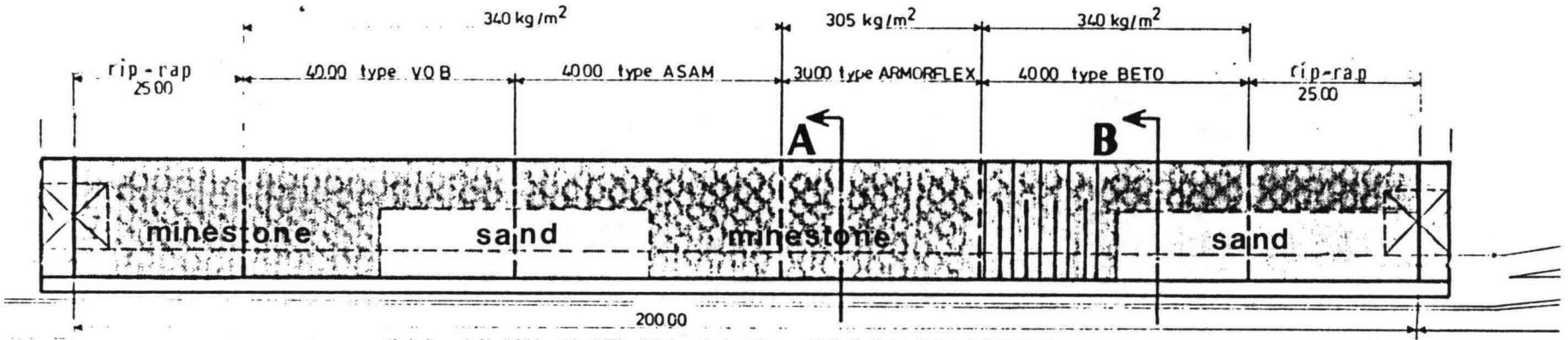


scale 1:1000

## SITUATION BANK PROTECTION

Fig. 3.2 Lay-out of test embankments

The following mat types were selected for these tests (from south to north).

- V.O.B.-mat: concrete blocks fixed to a geotextile by synthetic pins. The blocks are fixed to the geotextile in a rectangular pattern. The connection between the blocks is secured by the geotextile.
  Standard sizes of the mat are 4 x 6 or 4 x 8 metres.

- Asam-mat: concrete blocks in "half-stone" bond, joined by 2 cables (stainless steel) per block and interlocked by cams. The shape of the blocks is a trapezium, in such a way that the top of each block is more or less horizontal after placing it on a slope.
  Standard size is 3 x 4 metres.

- Armorflex-mat: basicly the same idea as the Asam-mat, although the shape of the blocks is different (no trapezium). The concept was originally developed in the USA. The blocks applied in the tests were closed concrete blocks (open blocks, allowing vegetation are also possible).

- Beto-mat: basicly the same principle as the Armorflex-mat, the main differences being the shape of the blocks and the method of connection of the blocks with 2 steel cables per block.

Each of these systems is also presented in appendix 1 to this report.

## 3.3 DESIGN ASPECTS

The design aspects of the several types of bank protection are summerized only very briefly in this report. Only those aspects that are relevant for the understanding of the behaviour are mentioned here.

a) Stability top layer
   The wave conditions, calculated from fetch length and wind speed, that are taken as the design load amount:
   - significant wave height $H_s$ = 1.2 m
   - mean wave period $T_z$ = 4.0 sec.
   The slope of the revetment is taken at 1 on 4 (vertical:horizontal).

   The resulting stone weight for rip-rap of natural stone with a density of 2700 kg/m3 amounts 650N.
   For the reference sections at both sides of the test sections a mixture of 10-300 kg (100-3000 N) unit stone weight has been taken.

For the mat sections the following weights were taken:
- VOB-mat : total weight 340 kg/m2
- other mats : total weight 305 kg/m2.

The following specifications can be summarized as follows:

| embankment type | thickness toplayer D | relative density $\Delta$ | $\Delta$ D |
|---|---|---|---|
| rip-rap | ~ 0.40 m | 1.7 | 0.68 |
| V.O.B. | 0.15 m | 1.2 | 0.18 |
| ASAM | 0.17 m | 1.2 | 0.20 |
| Armorflex | 0.15 m | 1.2 | 0.18 |
| Beto | 0.17 m | 1.2 | 0.20 |

The interstices between the blocks were not filled with gravel.
The stability factor for the block mats $H_s/\Delta D$ amounts 6.0-6.7. This is a high value compared to the standard criterion of $H_s/\Delta D = 4$.
The reason of this is twofold:
a) some calculation and laboratory test results showed that $H_s/\Delta D = 4$ is conservative;
b) the availability of the mattresses: for each type the maximum standard dimensions were selected.

b) Filter stability
Under all mats a geotextile has been applied to prevent washing out of fine materials through the gaps between the blocks (especially of the Asam, Armorflex and Beto types).

Under the geotextile a layer of minestone 10/250 mm has been applied, to be placed on top of the sandy core of the dike.
In the design stage some doubt existed on the possibility of the penetration of sand from the core into the filter layer. For this reason inspection of the filter layer in the evaluation stage at the end of the test programme was foreseen.
At a part of the test sections the geotextile was placed directly on the sand at the upper part of the slope (above mean water level).

To prevent water overpressure in the filter the permeability has to increase going from the core to the top layer.
This aspect has been one of the design criteria for the geotextile.

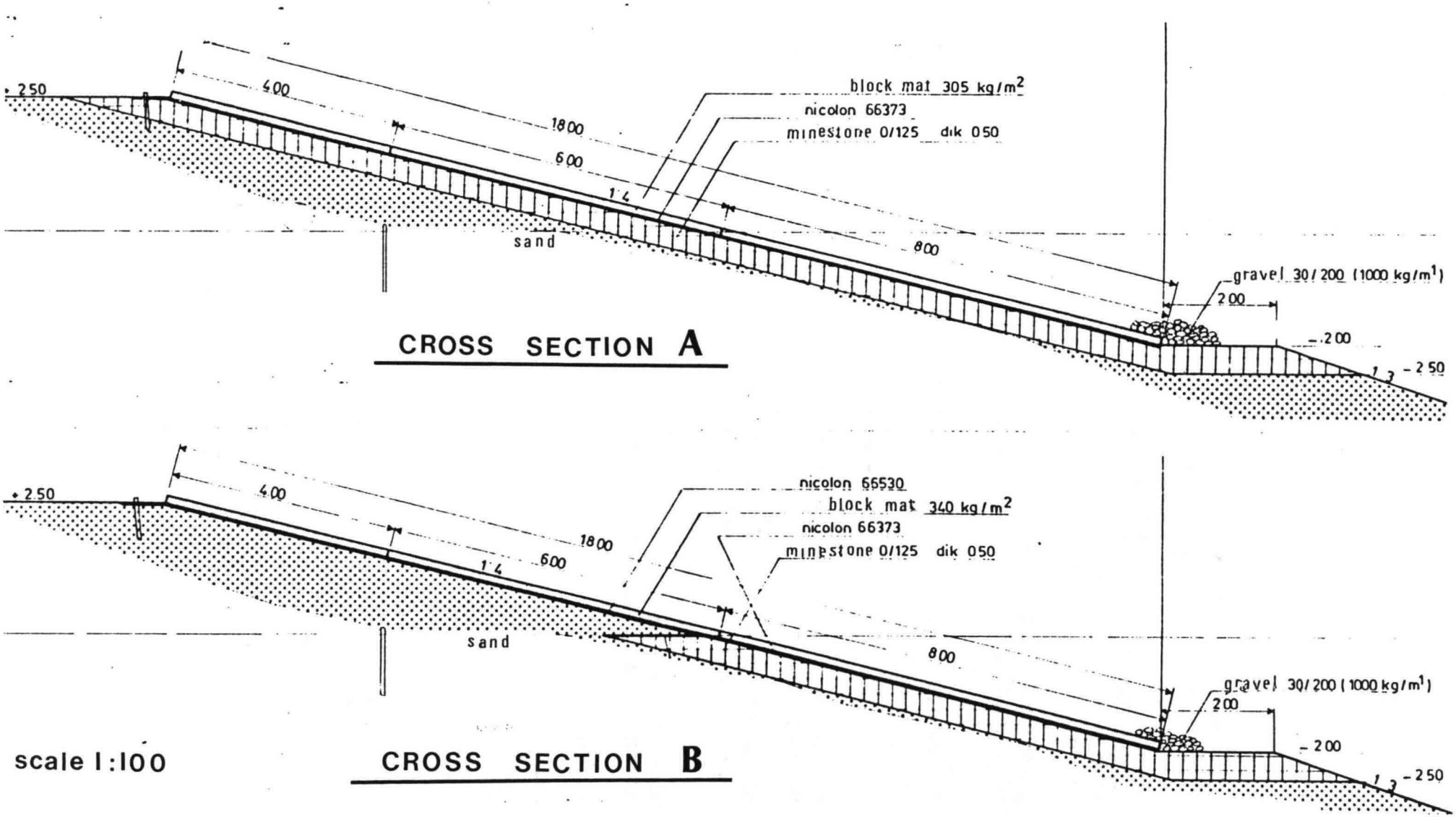


Fig. 3.3 Typical cross sections of the test embankments

c) Stability subsoil
For reasons of stability of the subsoil a slope of 1 on 4 (vertical:horizontal) was selected.

d) Top of the slope protection
The top of the armoured slope was 2.5 m above the waterlevel for all types of block mats.
The top of the mats was fixed to wooden piles that were anchored in the core of the dike.

e) Toe of the slope protection
The toe level for all mat types was 2 m below the mean waterlevel. On this level a berm of 2 m width consisting of a minestone layer of 0.5 m thickness was constructed. On top of this layer gravel 30/200 mm was dumped (total weight 1000 kg per running metre).

f) Joints between the mats
The several mat types were connected to each other by means of cables of stainless steel winded around the end blocks of each mat type.
The geotextile underneath the mats was continuous at these joints.

Typical cross sections of the test embankments are given in figure 3.3.

## 3.4 DESCRIPTION OF THE TEST RESULTS

Immediately after completion of the test sections in September 1986 an automatical wave and waterlevel recorder was installed in front of the dike. This recorder was damaged the first week after installation by an unknown vessel.
Before re-installation of the recorder, at October 20th, 1986, approximately 1 month after completion of the test sections, a severe storm occured, causing damage to all mat types.
The (estimated) wave height during this storm exceeded the design conditions with some 30-40%.
This storm and the damage to the structure will be discussed in the next section.
After this storm a relatively quiet period followed, without any further damage until the end of the test period in 1989.

mats were not connected to each other

$\frac{5}{2,25} = 2,24$

$\frac{H_s}{SD} = \frac{1,2}{1,4 \cdot 0,17} = 5$

$\frac{1,2}{1,2 \cdot 0,17} = 5,88$

$L = 1,56 \cdot 25 = \frac{156}{4} \simeq 39\,m$

$\frac{H_s}{L} = \frac{1,7}{39} = \frac{1,7 \cdot 2,5}{100} \simeq 0,042$

$\xi = \frac{\tan \alpha}{\sqrt{H_s/L_0}} = \frac{1}{4} \frac{}{\sqrt{0,04}} = \frac{1,0}{4,2} \simeq 1,25$

$\frac{H}{SD} = \frac{\Phi}{\xi} = \frac{5}{1,25} = 4$

$\frac{4,375}{1,25} = 3,5$

## 3.5 THE STORM OF OCTOBER 20TH, 1986

a) Definition of hydraulic conditions
As already stated, the wave and waterlevel recorder failed at the day of the storm.
From other observations in the surroundings of the test location the following conditions could be derived:
- max. wind velocity (ghust): 29 m/s
- significant wave height $H_s$ = approx 1.7 m
- mean wave period $T_z$ = approx 5 sec.
- max. wind set-up of the waterlevel: approx. 1 m.

b) Visual description of the damage
After the storm all mat types were damaged.
The damage consisted of:
- downward displacements along the slope
- deformation of the slope
- damage at the joints between the different mat types, especially between the ASAM- and Armorflex mats the mat edges were turned-over
- damage at the internal joints between the standard mat sections of 4, 6 and 8 metres length.

Especially at the joints locally the geotextile underneath the matresses was visible.
An impression of the damage is given in Appendix 3 attached to this report.

The reference sections of rip-rap at both sides of the test sections were only slightly damaged.

c) Stability calculations
The wave characteristics during the storm were:
$H_s$ = 1.7 m
$T_z$ = 5 sec.
The corresponding wave breaking parameter reads:
$\xi_z$ = 1.20

The following $H_s/\Delta D$ values can be calculated now:

| type | $\Delta D$ [m] | $H_s/\Delta D$ [-] | $\phi$ *) [-] | f [-] |
|---|---|---|---|---|
| rip-rap | 0.68 | 2.5 | 2.05 | 0.82 |
| V.O.B. | 0.18 | 9.4 | 3.5 | 0.37 |
| ASAM | 0.20 | 8.5 | 3.5 | 0.41 |
| Armorflex | 0.18 | 9.4 | 3.5 | 0.37 |
| Beto | 0.20 | 8.5 | 3.5 | 0.41 |

*) including the effects of the slope angle and the wave breaking parameter.

For all mat types the stability factor f, being the ratio between strength ($\phi$-value) and load ($H_s/\Delta D$ value) is much less than 1.
It is obvious that failure of the slope protection is very likely in this case.
Some damage to the rip-rap sections is also likely.

## 3.6 DISCUSSION ON FAILURE MECHANISMS

The storm of 20th October 1986 caused such a high exceedance of the design loads that all mat types were seriously damaged.
These circumstances make it impossible to refine the stability criteria of these mat types on the basis of the experiments.
On the other hand, the high exceedance of the design loads resulted in a number of failure mechanisms, that occured simultaneously.
The following mechanisms could be observed after the storm:

- lifting up of the mats, both of individual blocks and of groups of blocks. This phenomenon leads to pulling forces in the connections between the blocks (cables or geotextile) and to deformation of the subsoil;
- loosening of the connection between 2 adjacent mat sections, as a result of the increasing forces when (part of) the mat is lifted up;
- sliding down of the mats as soon as the connection between 2 adjacent mat sections has failed. Sliding may take place between the geotextile and the subsoil and also between the blocks and the geotextile (the latter for the types without block to geotextile fixation);
- turning over of mat ends, especially after failure of the connection between adjacent sections; according to the design rules open mat ends without any anchoring or connection should be treated as a single block;
- bobbing up of the mats at the downward end of a mat section that has been lifted, resulting in an ongoing sliding down process;
- breaking of steel cables, causing a loss of the internal connection of a mat section; the blocks act as single stones then, with much lower stability level;
- erosion of the toe material, consisting of gravel 30-200 mm (1000 kg/m') on minestone. The toe level was some 2.5 m below the still water level during the storm, being too high to withstand the wave forces;
- erosion of the sublayers, starting from holes in the slope protection and from the eroded toe.
  This erosion was observed at the sections where the geotextile was placed directly on the sand and also at the sections where a 0.5 m thick layer of minestone was applied, although the extent of the erosion in the latter situation was less.

In the Hartel Canal the spaces between the blocks of the mat systems were filled in with gravel. At the Houtrib-dike this fill was not applied.
In view of the damage that has been observed, it can be doubted whether this default has led to a more severe destruction or not.
In general terms, it seems to be likely that filling in of the interstices by gravel indeed raises the level of incipient instability.
However, as soon as significant displacements take place in spite of the gravel fill, the fill will probably be washed out soon and the mat stability will switch down to levels corresponding to open interspaces.

This example shows clearly that a very careful analysis with respect to the "secondary" stability criteria of the mat system itself (joints, filters, toe, lifting/sliding, etc.) and also with respect to the structure related aspects (extent of damage, costs and time required for repair, consequential losses, etc.) is deemed to be necessary before making a decision on the stability level to be accepted, especially for advanced systems that have a high resistance against wave attack.

## 3.7 CONCLUSIONS

All 4 mat systems that were applied at the Houtrib-dike were seriously damaged.
In view of the hydraulic loads that occured during an extreme storm on 20th October 1986, the damage was not exceptional.

As the storm happened to come immediately after completion of the test embankments, no experience could be obtained about the behaviour of the mats under moderate conditions.

The observed damage demonstrated the presence of a number of failure mechanisms, most of them being related to each other.

The most important lesson of the tests at the Houtrib-dike is that the weakest point of block mats is the joint between 2 adjacent mat sections.

# DUTCH PROTOTYPE EXPERIMENTS WITH BANK PROTECTION SYSTEMS

Appendix 1

Photographs of tested slope protection systems

fine gravel (30-80 mm) on geotextile on sand (Hartel Canal)

coarse gravel (80-200 mm) on geotextile on sand (Hartel Canal)

rip-rap (5-40 kg) on geotextile, both on clay and on sand (Hartel Canal)

blocks placed on geotextile, clay, on gravel and on sand (Hartel Canal)

Basalton blocks placed on silex and on geotextile/sand (Hartel Canal)

Armorflex block mats placed on gravel (Hartel Canal)

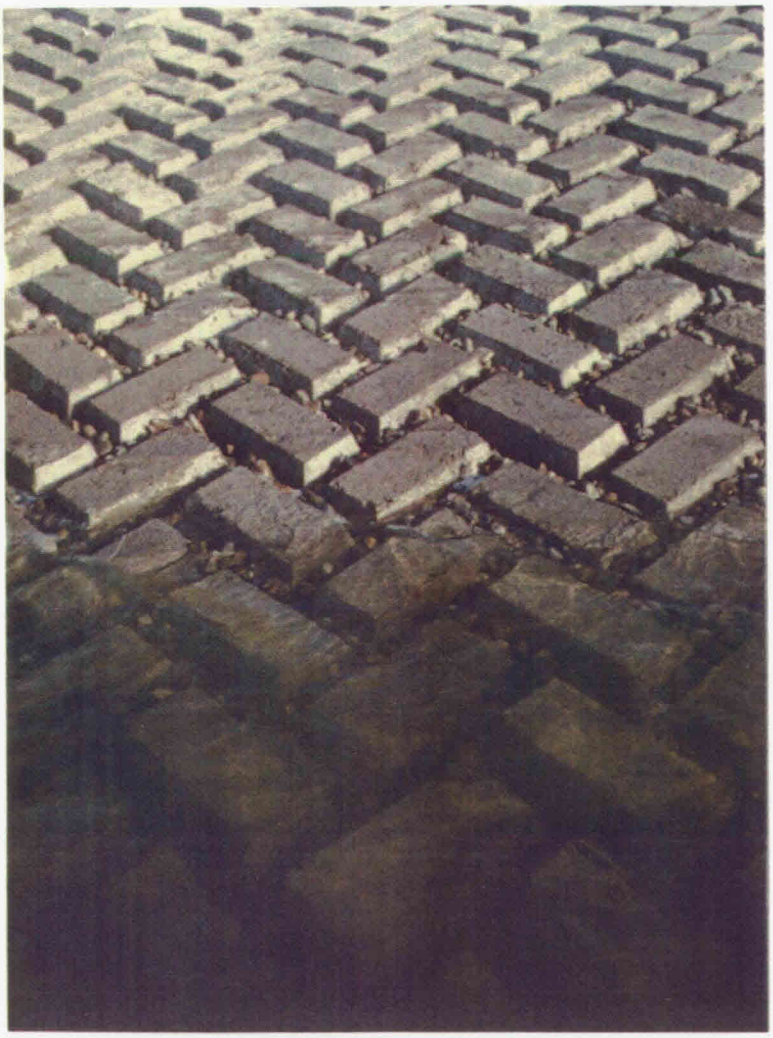

ACZ-Delta block mats placed on geotextile/ gravel (Hartel Canal)

sand-sausage mattress Profix placed on gravel (Hartel Canal)

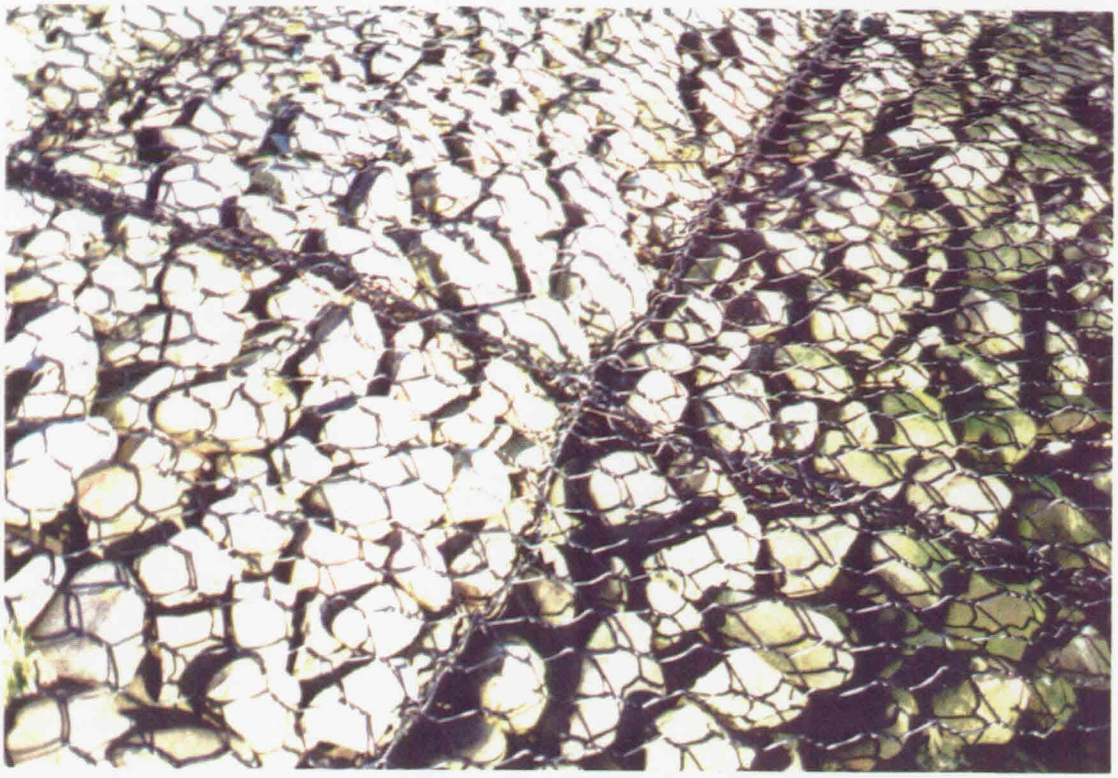

PVC-Reno mattress (Maccaferri Gabions) placed on geotextile on sand (Hartel Canal)

Fixtone open stone asphalt placed on sand asphalt on sand Hartel Canal

V.O.B.-mat, fixed to a geotextile and placed on minestone and on sand (Houtrib-dike)

ASAM-mat, placed on a geotextile on minestone and on sand (Houtrib-dike), showing joint between 2 adjacent mat sections

Armorflex-mat placed on a geotextile on minestone (Houtrib-dike), showing joint between 2 adjacent mat sections

Beto-mat placed on a geotextile on minestone and on sand (Houtrib-dike), showing joint between 2 adjacent sections

NOTE: The last 4 pictures (Houtrib-dike) were taken after the storm; the performance immediately after completion was much better

# DUTCH PROTOTYPE EXPERIMENTS WITH BANK PROTECTION SYSTEMS

Appendix 2

Design of bank protection of inland navigation fairways

# design of bank protection of inland navigation fairways

presented at the International Conference on Flexible Armoured Revetments Incorporating Geotextiles, London, England, 29–30 March 1984

H.G. Blaauw, F.C.M. van der Knaap, M.T. de Groot and K.W. Pilarczyk

publication no. 320

June 1984

# DESIGN OF BANK PROTECTION OF INLAND NAVIGATION FAIRWAYS

H.G. BLAAUW and F.C.M. van der KNAAP, Delft Hydraulics Laboratory, M.T. de GROOT, Delft Soil Mechanics Laboratory, and K.W. PILARCZYK, Hydraulics Division, Rijkswaterstaat

SYNOPSIS.
The collapse mechanism of bottom and bank constructions of fairways under attack of ship induced water motion has been studied from model and prototype tests. Transport relations and design criteria for subsoil, filter layers, and protection layers consisting of rip rap or blocks are formulated and verified, as far as they are at present.

## INTRODUCTION

1. Ships sailing in inland navigation fairways, produce a water motion which attacks the bottom and banks. During recent years power and ship size has increased considerably, resulting in more intensive attacks of fairway boundaries and, thus, to high maintenance and construction costs. Due to these reasons, the Dutch Public Works has charged the Delft Hydraulics Laboratory (DHL) with a long-term investigation to develop design rules for bank and bottom protection.

2. A protection layer should resist the hydraulic attack and at the same time prevent the movement of subsoil and/or filter material through the construction. Also, sliding of the subsoil or parts of the construction must be prevented. Both hydraulic and geotechnical aspects are thus of importance, and therefore, the investigations are being carried out in close cooperation with the Delft Soil Mechanics Laboratory (DSML).

3. Two basic design approaches can be identified: the deterministic and the probabilistic. In the deterministic approach a dominant design condition is selected. On the basis of this condition the dimensions of the protection layer and filter are determined for the criterion of 'initiation of motion' (1. no (or slight) displacement of individual stones of a rip rap top layer can be accepted; 2. lifting of individual blocks of a block revetment by pressure forces perpendicular to the slope cannot be accepted). The probabilistic approach aims at a calculation of the total damage of the construction on, for instance, a time (year)

base. The transmission functions required for this type of calculation are determined by means of deterministic tests. The present paper is therefore restricted to deterministic design rules. The transport relations, required for a probabilistic approach, will be presented as far as they are, at present, available.

4. The investigations carried out, in the prototype and also at a reduced scale, mainly concern push-tow canals, bank slope 1:4, a rip-rap protection and a geotextile or granular filter. Studies into the behaviour of block revetments have started recently, and some initial results are discussed.

## DESIGN PROCESS

5. The design process, as presented in Fig. 1, forms the basis of the design technique adopted.

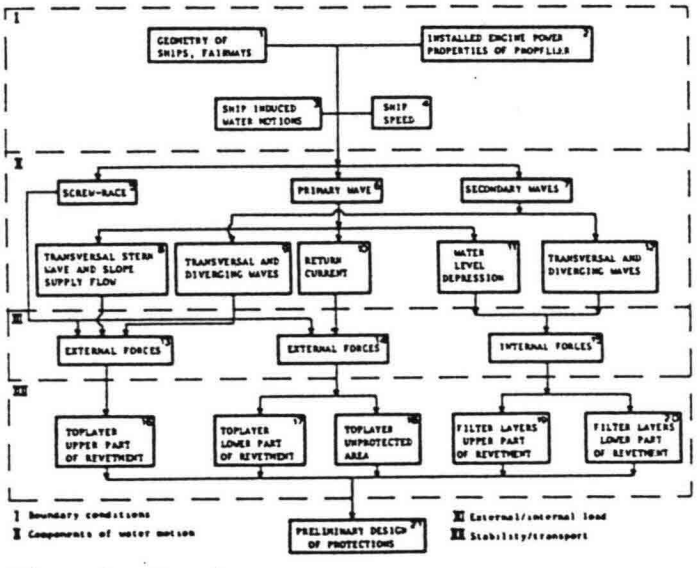


Fig. 1: Design process

The ship-induced water motion and the corresponding ship speed are calculated (Blocks 1 through 7) using known ship dimensions, fairway cross-profile, and applied engine power.

6. The ship-induced water motion can be split up into screw race, primary wave and secondary waves (Blocks 5, 6, 7). The primary wave components are: return current, water-level depression, front wave, transversal stern wave (Blocks 8, 10, 11).The secondary waves are composed of diverging and translating waves which together form the well-known interference peaks. These waves are indicated in Blocks 9 and 12.

7. The various components of the ship-induced water motion are indicated schematically in Fig. 2.

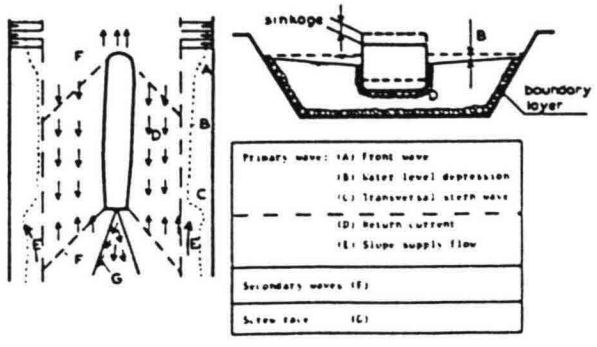


Fig. 2: Review of water motion components

8. The ship-induced water motion attacks the fairway boundaries. Basically the areas under attack, see Fig. 3, are: (a) unprotected bottom and part of the banks, (b) lower protected area, and (c) upper part of revetment. The return current (and screw race) are important, for Areas a. and b., whereas secondary

waves and/or transversal stern wave dominate in Area c.

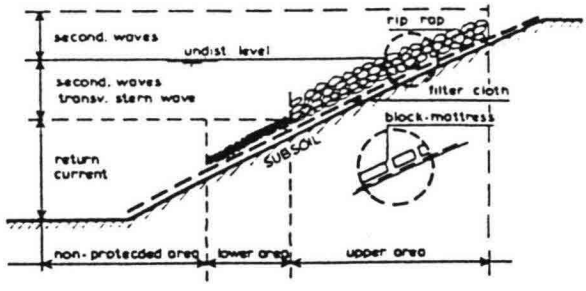


Fig. 3: Areas in the canal cross-section and dominant component of the water motion

9. The external loads (transversal stern wave, secondary waves, return current) exert friction and pressure forces on the protective layer and are of prime importance for the determination of dimensions of this layer. In the subsoil the pore pressures respond to external variations of the water-level (front wave, water-level depression, secondary waves). The resulting forces determine the design requirements for the filter.

## HYDRAULIC LOAD

### General

10. Detailed calculations of the ship-induced water motion, based on the given geometry of a fairway cross-profile, the ship and the applied engine power are elaborated in this chapter.

11. In addition to the ship-induced water motion other hydraulic phenomena occur such as wind waves and tidal current. In the fairways considered in the present studies ship-induced waves are more important than wind-induced waves. Therefore the wind-induced waves have not been taken into account particularly in case of a deterministic design. The effects of both ship-induced currents and natural currents are discussed.

### Speed prediction

12. Frequently vessel speed prediction calculations are not required since the velocities of various types of ships are well known. For instance in case of the renewal of an existing protection (or large- scale maintenance) the design can be based on the existing conditions. However these calculations are indispensible, for new fairway design and/or introduction of new vessel shapes or more highly powered ships.

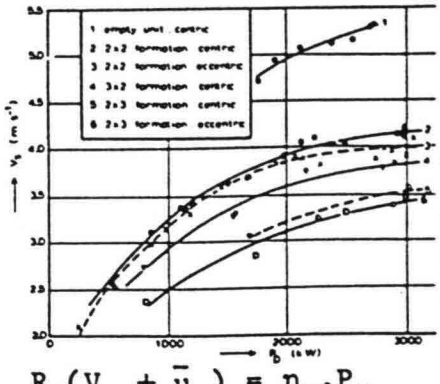


Fig. 4: Relation between shaft-horse power and ship speed

13. Speed prediction calculations are based on the equilibrium of the total required power, on the one hand, and part of the shaft horsepower, representing the thrust power, on the other, viz:

$$R_T(V_s + \bar{u}_r) = \eta_D \cdot P_S \qquad (1)$$

In ref. 1 this relation is extensively elaborated for pushing convoys.

14. Measurements of resistance and propulsion were carried out during the first series of tests on the Hartel-canal in 1981 for several configurations of pushing convoys. It follows that, for loaded convoys: $\eta_D = 0.85$ . The relation between shaft-horse power and ship speed for investigated types of convoys, are given in Fig. 4.
It clearly follows, that the speed tend to limiting values for higher applied powers.

General ship-induced water motion

15. The calculation of the ship-induced water motion is very complicated and due to the full form of most of the ship types the presence of bottom and banks, and the free water level a three-dimensional calculation is necessary. This type of calculation has not been fully developed yet and for the presentpaper only a series of (most) one dimensional calculation methods are discussed.

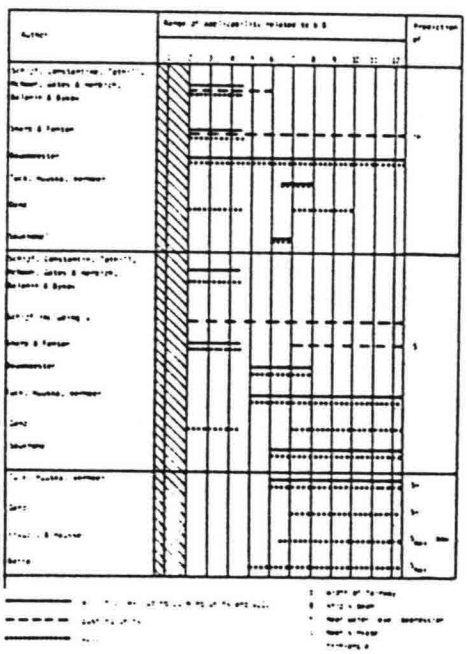

Fig. 5: Survey of results

16. Generally, three main approaches can be distinguished, based on: conservation of energy, or momentum (one-dimensional; two-dimensional slender body theory; empirics. To get insight into the applicability of these methods, a thorough investigation was carried out, at the DHL, to determine which calculation method can best be used as function of width restriction of the fairway and ship type. These investigations are reported in ref. 2. The methods were verified with respect to their applicability to predict water-level depression, sinkage and, if possible, squat.

17. The results presented in ref. 2 were recently extended with results of prototype measurements (ref. 3). A survey of results is given in Fig. 5.
For the calculation of areas of water-level depression it follows that, for pushing units, the method of Sharp and Fenton gives relatively good results, while for other ship types (including VLCC) the method of Bouwmeester proved to be satisfactory.

Detailed ship-induced water motion

18. Return current. The maximum return current ($0_r$) and the simultaneously occurring maximum shear stress ($\hat{\tau}$) are decisive for the stability of a bank or bottom protection. During the conditions observed the return current had a more

or less uniform distribution outside the boundary layers of ship and bottom, and banks. The current direction coincided approximately with the direction of the fairway axis (ref.5).

19. The shear stress can be calculated according to:

$$\hat{\tau} = c_{fr} \tfrac{1}{2} \rho \hat{u}_r^2 \text{ in which } c_{fr} = (2.87 + 1.58 \log \frac{x}{k_s})^{-2.5} \qquad (2)$$

according to the Schlichting Formula for rough plates.
In this formula x is the distance over which a water particle near the embankment has moved due to the return current when a certain part of the ship-length (X) has passed. x is given by:

$$x = \frac{\bar{u}_r}{\bar{u}_r + V_s} X \qquad (3)$$

The maximum value for $\hat{u}_r$ occurs at a distance of 0.25 to 0.35 $L_{OA}$ from the bow.

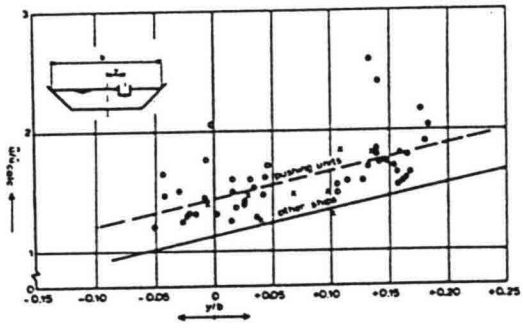

Fig. 6: Relation between extreme and average return current

The value for the bottom roughness ($k_s$), including effects of unevenness, had quite a spread. A value of $k_s = 4.D_{50}$ is an acceptable average value.

In Fig. 6 the value of $\hat{u}_r$, related to $\bar{u}_r$ for a certain ship speed, can be taken as function of rate of "eccentricity"(y).

20. When a natural current prevails, in the fairway, the shear stress due to the return current ant the natural current can be calculated, according to ref. 4:

$$\tau = \tfrac{1}{2} c_{fc} (u_c + \sqrt{\frac{c_{fr}}{c_{fc}}} \hat{u}_r)^2 \text{ in which } c_{fc} = 0.06 \{\log \frac{12h}{k_s}\}^{-2} \qquad (4)$$

21. Transversal stern wave. The principal characteristics of

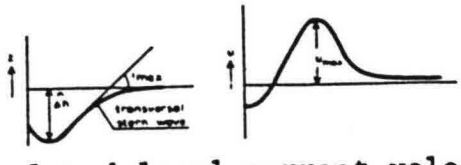

Fig. 7: Principal characters of transversal stern wave

the transversal stern wave and related local current velocities at the side slopes are indicated in the sketch presented in Fig. 7.

22. The steepness of the transversal stern wave has been determined at both model and prototype scales. It follows from

$$i_{max} = (\frac{\hat{\Delta h}}{z_o})^2 \qquad (5)$$

The steepness has a limiting value of $\hat{i}_{max} = 0.1$ to 0.15.
The factor, $z_o$, can be calculated according:

$$\frac{z_o}{b} = 0.04 - 0.158\,\frac{y}{b} \qquad (6)$$

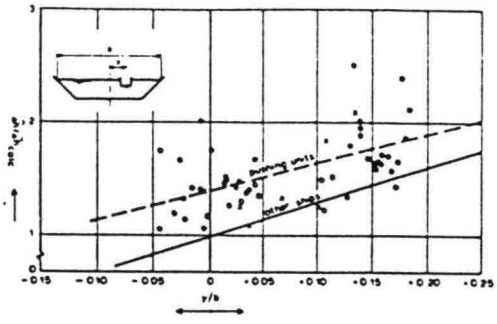

Fig. 8: Relation between transversal stern wave height and average water-level depression.

Taking into account the effect of "eccentric" navigation (y/b). The maximum value of the height of the transversal stern wave related to the results of the one-dimensional calculations ( $\overline{\Delta h}$ ), including the effect of "eccentric" navigation, is given in Fig. 8.

23. The maximum current velocities occurring in the transversal stern wave can be estimated as:

$$u_{max} = 0.1 \text{ to } 0.2\ V_s, \text{ if } \hat{\Delta h}/\Delta.D_{50} < 1 \text{ and}$$
$$u_{max} = \left(1 - \frac{\Delta.D_{50}}{\hat{\Delta h}}\right) V_S, \text{ if } \hat{\Delta h}/\Delta.D_{50} > 1 \qquad (7)$$

24. Secondary waves. Secondary waves are composed of transverse and diverging waves, which together form interference peaks. Interference peaks, and, to a less extent (behind the ship) transverse waves are of special interest in relation to bank attack. Secondary waves are elaborated thoroughly in ref.7. A relation has been derived to determine the height of the interference peaks using the method of Gates and Herbich (ref. 8):

$$H_i = \alpha_i.h.\left(\frac{S}{h}\right)^{-0.33} . \left(\frac{V_s}{\sqrt{gh}}\right)^{2.67} \qquad (8)$$

From DHL prototype and model experiments it follows that: $\alpha_i$ = 0.80, pushing unit (loaded); $\alpha_i$ = 0.35, pushing unit (empty), tugboat; $\alpha_i$ = 0.25, conventional inland motorvessel. The wave length of the interference peaks can be described, ref. 7, as:

$$L_{wi} = 0.67 \cdot \frac{2\pi}{g} \cdot V_s^{\,2} \qquad (9)$$

25. Screw race. The velocities occurring in the screw race for ships manoeuvring and underway are extensively dealt with in ref. 9 and ref. 10. For a manoeuvring ship the velocities behind the propeller can be calculated according:

$$\frac{u_{x,r}}{u_o} = \frac{2.8\ D_o}{x_s} \cdot \exp\left[-15.4\,\frac{r^2}{x_s^2}\right] \qquad (10)$$

with: $D_o = 0.71\ D_p$ (propeller); $D_o = D_p$ (ducted propeller); $D_o = 0.85\ D_p$ (propeller in tunnel).
The limited outflow velocity is

$$u_o = 1.60 \cdot n_p \cdot D_p \cdot \sqrt{K_{TP}} \qquad (11)$$

The influence of forward ship speed, presence of rudders and the consequences of the operation of more than one propeller are discussed in (ref.10).

26. Front wave. On the basis of the results of prototype and model experiments, the steepness of the front wave at the bank slope can be obtained from:

$$i_f = c(y) \cdot \Delta h_f \text{ in which} \qquad (12)$$

$$c(y) = 4.06 \cdot 10^{-4} \cdot y + 1.79 \cdot 10^{-2} \qquad (m^{-1})$$

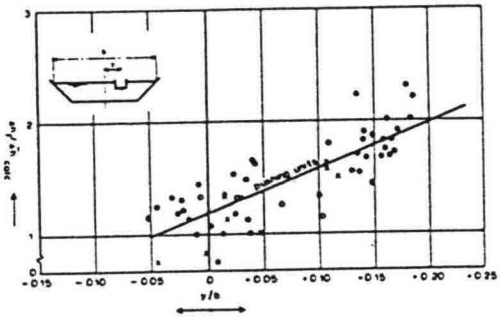

Fig. 9: Relation between front wave height and average water level depression

The height of the front wave, related to the calculated water level depression, is presented as function of the rate of "eccentric" navigation (y/b) in Fig.9. The front wave is important for the determination of the prevailing pressure gradients in the subsoil.

INTERNAL LOAD

27. Ship-induced waves in a channel constitute a direct external hydraulic load on the embankment but also bring about, indirectly, an internal load. Fluctuations in the water level due to passing ships affect pore water pressures under the top layer of the bank protection and in the subsoil. The influence of the fluctuations depends on wave frequency and amplitude and also on design characteristics, such as geometry of filter layers and on the permeability, density and stiffness parameters of the subsoil.

28. Wave-induced pore pressures under the revetment layer and in the subsoil constitute the internal load on the bank protection structure. The relation between external and internal loads plays an essential role when considering the strength of the bank protection, and the stability of bank protection can only be determined satisfactorily by considering the top layer and subsoil simultaneously. Optimizing a design only with respect to, say, maximum strength of the top layer against the external load, can give rise to loss of internal stability and thus lead to erosion. Meeting the requirements for external stability does not automatically imply internal stability or vice versa. In some cases a compromise has to be found see, for example, section 35.

29. Hydraulic boundary condition. Only fluctuations of the water-level will form the representative hydraulic boundary condition for the internal load. Both amplitude and speed of these fluctuations have an impact on the induced groundwater flow.

30. Response subsoil. In general the response in the subsoil to channel water-level fluctuations can be described as follows. The phreatic level in the filter layer(s) cannot immediately follow a sudden lowering of the channel level.

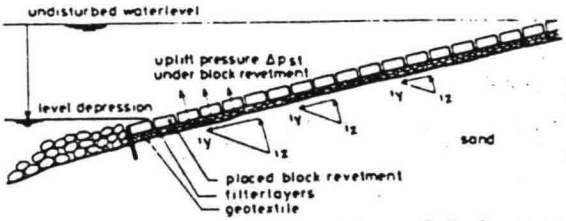


Fig. 10: Wave-induced internal load factors

Under the top layer of the protection there remains an excess pore pressure, which results in hydraulic gradients in three main directions: (a) a hydraulic gradient, $i_x$, in the longitudinal direction of the waterway, (b) a hydraulic gradient, $i_y$, in the transverse direction of the waterway in the plane of the slope, and (c) a hydraulic gradient, $i_z$, in the direction perpendicular to the slope. Furthermore, uplift pressures, $\Delta p_{st}$ against the slope revetment occur, when there are less permeable top layers, see Fig. 10.

31. Prototype measurements. An attempt has been made to establish a relation between he external hydraulic load and the induced internal load factors using a theoretical approach (analytical, numerical), see section 62, a scale model approach, see ref. 6, and prototype measurements. Prototype measurements have been carried out in the Hartel-canal in the harbour area of Rotterdam in 1981 and also very recently in 1983. External and internal loads induced by pushing units have been thoroughly investigated; several types of bank protection served as test sections for the experiments, see ref. 11.

32. Relation between external and internal load. Both the leading limits of the water-level depression (front wave) and its gradient with respect to time are representative for the internal load. Results of prototype measurements show, that the product of the front wave height $\Delta h_f$ and the speed, with which the water level depression comes about is a satisfactory practical measure for the internal hydraulic gradients. Note, that the ship's speed $V_s$, is implicitly represented by the quantity $\Delta h_f \cdot \frac{\partial h}{\partial t}$, viz.:

$$\Delta h_f \cdot \frac{\partial h}{\partial t} = \Delta h_f \cdot \frac{\partial h}{\partial x} \cdot \frac{\partial x}{\partial t} = \Delta h_f \cdot i_f \cdot V_s \qquad (13)$$

33. The hydraulic gradient, $i_x$, in the longitudinal x-direction, proved to be only of minor importance in the relation between internal load and strength. Any grain transport in this direction can be either positive or negative depending on the navigation direction. Generally the net grain transport in the x-direction can therefore be neglected. On the other hand, in the transverse direction, the internal response to the external load is of particular interest.

34. Figures 11, 12 and 13 show, for three types of protection, the measured transverse hydraulic gradient, $i_y$,

directly under the geotextile as a function of the compound hydraulic boundary condition, $\Delta h_f \cdot \frac{\partial h}{\partial t}$. It follows, that application of a relatively permeable gravel layer under the top layer of concrete blocks reduces transverse hydraulic gradients considerably. Apparently the storage capacity of the gravel layer allows flow from the subsoil through the geotextile into the filter layer, thus reducing flow under the geotextile towards the toe of the slope. Figures 11, 12 and 13 show a more or less linear increase of the transverse hydraulic gradient, $i_y$, with $\Delta h_f \cdot \frac{\partial h}{\partial t}$ up to a value of $\Delta h_f \cdot \frac{\partial h}{\partial t}$ in the range 0.01 to 0.02 $m^2/s$; above this value almost no further increase in $i_y$ was measured. Maximum values for $i_y$, in the order of 0.5, were recorded for concrete blocks without an underlying gravel layer. This maximum value was attained at the lowest outcrop point of the groundwater,

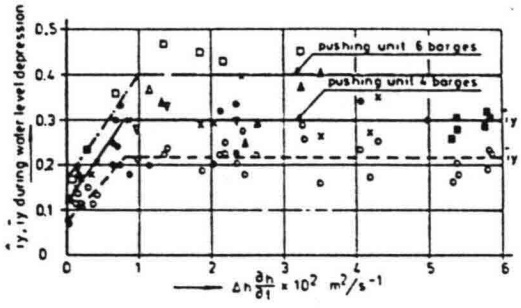


Fig 11 Test section of placed block revetment upon gravel layer

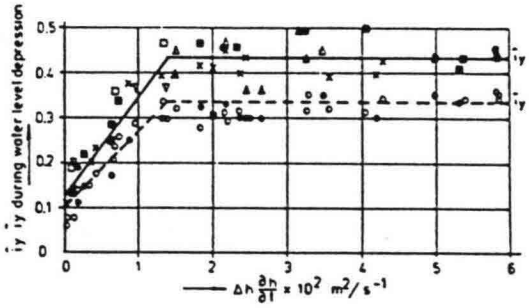


Fig. 12 Test section of placed block revetment

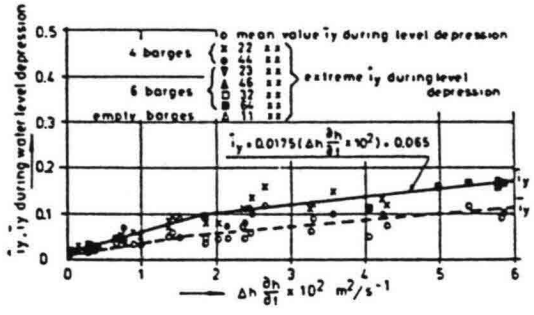


Fig. 13: Test section of rip-rap

following a water-level depression. Since, in general, the amount of pore water in a slope is large with respect to the flow discharge into the channel during a water-level depression, the transverse hydraulic gradient, $i_y$, will continue to be operative as long as the passage of the ship.

35. Hydraulic gradients, $i_z$, measured perpendicular to the slope, were very similar for the different test sections. The value of $i_z$, averaged over the upper first half a meter perpendicular to the slope was about 0.15. These uplift gradients occurred during the channel water depression, that is, simultaneously with the transverse gradient, $i_y$. Ref. 12 shows that this combination of "blowing" (flow in an upward direction) with flow parallel to the surface is more critical for grain stability than suction with flow parallel to the surface. Although blowing reduces the effect of the drag force exerted by the parallel flow, the reduction of the

effective grain weight is the principle unfavourable factor contributing to loss of grain stability.

36. Uplift pressures under the top layer, as a consequence of a fall in the water-level, are to be expected in the case of revetments which are only slightly permeable, for example, concrete blocks laid with very narrow joints. Such a

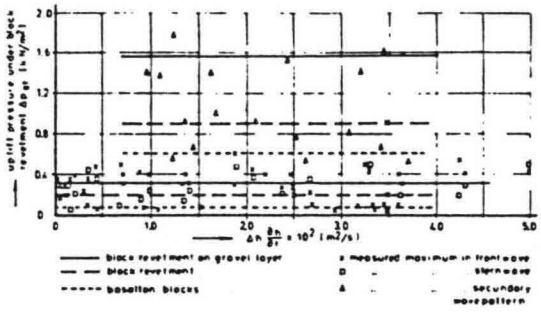

Fig. 14: Uplift pressures under block revetment

protection, with joint width smaller than 0.5 mm, has been examined in the Hartel-canal prototype measurements. Uplift pressures, $\Delta p_{st}$ are shown in Fig. 14. Here there is a conflict between the design for external stability and the design for internal stability. Application of a gravel layer under the revetment increases uplift pressures but reduces transverse hydraulic gradients directly under the geotextile. Making therevetment more permeable, within limits, by enlargingthe joints can possibly balance these conflicting design requirements.

37. The prevailing question about whether the magnitude of internal hydraulic gradients and uplift pressures will lead to loss of internal stability is connected with the relation between internal loads versus strength of the protection. Although complete answers cannot yet be given some aspects are discussed below in section 38 and following.

## STRENGTH OF BANK CONSTRUCTION

### Technical requirements

38. The technical requirements can be described briefly as follows: a good construction must be sufficiently stable, flexible and durable. Stability means that no part of the construction can be displaced (see Introduction); flexibility, on the other hand, means that the construction (or part of it) can deform to a limited extent without losing mutual connection. Durablity concerns the resistance of the materials to weathering of any kind.

### Internal failure mechanisms

39. The stability of bank protection can be endangered by external forces, and by the induced internal forces. It is desirable to determine critical values for typical internal load factors, which, in turn, depend on the external hydraulic load. The criterion for such critical values should be, that internal loads exceeding this value lead to erosion of whatever kind. The kind of erosion depends to some extent on the type of bank protection. Questions that arise immediately are: what internal load factors can be taken as typical; what failure mechanism, brought about by the typical internal load, does one have in mind; how can one provide against possible internal erosion. Formulation of such

critical values for internal load factors provides an essential tool for developing design criteria for bank protection.

40. In the case of placed block revetments, initially there is a loss of stability when induced uplift pressure forces exceed the sum of the weight of single blocks and their mutual friction forces. One or more blocks can be lifted out from the revetment and the external hydraulic load can then act freely upon the protection, accelerating failure. To rely on uncertain friction forces is hazardous, since the uplift of one single block can lead to extensive damage of the protection. With blocks which do not interlock one has to take into consideration that some blocks in the revetment will be badly connected. In addition uplift pressures under neighbouring blocks will reduce any friction effects considerably. Both prototype measurements and analytical models, ref. 13, 14, and 15, show, that uplift pressures increase with the permeability of the subsoil filter layer and decrease with the permeability of the top layer.

41. The stability of block revetments can also be endangered when hydraulic gradients, $i_y$ and $i_z$, on the interface between top layer and subsoil exceed the critical value. Depending on the storage capacity of the subsoil grain transport can take place through the geotextile or towards the toe of the slope, see Fig. 15. To provide against this long-term failure mechanism a sandtight geotextile should be placed on the subsoil. The determination of critical values for the internal load is being studied in the laboratory.

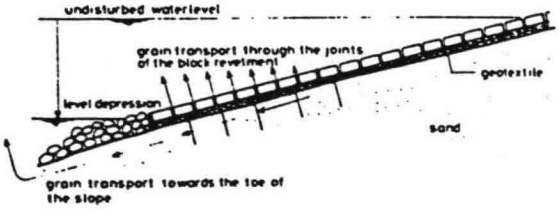


Fig. 15: Possible failure mechanisms by internal load

42. Design. For a filter to function properly it has to meet requirements for sandtightness and water permeability. Recent research for the storm surge barrier in the Eastern Scheldt indicates that vertical, parallel, cyclic and stationary flows can be distinguished in granular filters, see ref. 16. Critical hydraulic gradients have been found to be higher for stationary gradients due to the arching of grains. Furthermore, the permeability of the filter layer or geotextile should be at least as high as that of the subsoil. The percentage of open area of the geotextiles, usually defined by the diameter $O_{95}$, is of specific interest. Although there is no uniformity for the limiting value of this parameter, $\frac{O_{95}}{d_{90}} < 2$ is considered to be on the safe side, see ref 17.

Stability and transport prediction for rip rap top layers

43. A number of computational models have been developed

from the analysis of experiments in order to predict the stability and the transport of the top layer material under attack of the return current (including natural currents), the transversal stern wave, the secondary waves and the screw race of the top layer.

44. Return currents and/or natural currents. The stability against currents can be computed in different ways. If the current velocity, $u_c$, near the bank is known a quick estimate can be made with the stability criterion according to (ref. 18) using:

$$\frac{u_c}{\sqrt{g.\Delta.D_n}} = k_1 \quad (= \text{a constant}) \tag{14}$$

From analysis of experiments it follows that $k_1 = 1.2$ to $1.5$

45. A more accurate estimate of the stability against currents can be made with the criterion of Shields (ref. 19). In this case the maximum shear stress, $\hat{\tau}$, acting on the rip rap has to be known in order to compute the flow parameter, $\phi$, from the following:

$$\phi = \frac{\hat{\tau}}{\rho.g.\Delta.D_{50}} \cdot \frac{1}{k_D} \quad \text{in which } k_D = \cos\alpha \sqrt{1 - \frac{\tan^2\alpha}{\tan^2\varepsilon}} \tag{15}$$

Different values of $\phi$ can be taken depending on the requirements, viz.: $\phi < 0.03$ - practically no transport of rip rap; $0.03 < \phi < 0.06$ - small transport of rip rap; $\phi > 0.06$ - rapidly increasing transport intensities.

46. In some situations some transport of material, caused by extreme loads, can be accepted. Such transports can be quantified with a modified version of the transport formula according to Paintal (ref. 5):

$$\phi = 1.64 \cdot 10^{10}\, \phi^{10.86} \tag{16}$$

in which $\phi$ = transport parameter, $q_s/\sqrt{g.\Delta.D_{50}}$, with $q_s$ representing the transport of material per unit width. Equation 16 is compared with measured transport data in Fig. 16.

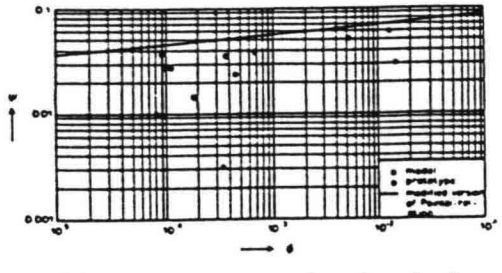

Fig. 16: Transport caused by return current

47. Transversal stern wave. The stability of rip rap on a slope 1:4 against the action of the transversal stern wave caused by a push tow unit sailing near to the bank has been determined. In Fig. 17 the measured number of transported stones ($n_{meas}$) has been plotted versus the characteristic stern wave parameter $\hat{\Delta h}/\Delta.D_{50}$. Clearly it can be seen that rip rap did not move when:

$$\frac{\hat{\Delta h}}{\Delta.D_{50}} < 2.3 \tag{17}$$

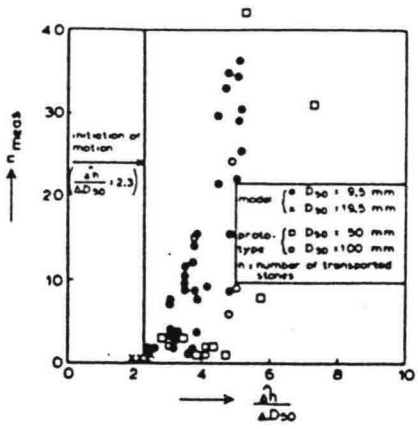

Fig. 17: Measured transport versus stern wave parameter

48. Two methods have been developed to predict the transport caused by the transversal stern wave of a push tow unit. The first method is the most simple and has been based on measurements of shear stresses caused by a solitary wave. From the measurements of Naheer (ref. 20) it can be shown that:

$$c_{fw} = 0.62 \frac{g.D_{50}}{v_s^2} \tag{18}$$

The flow parameter $\phi_w$ can be determined from Equations (7) and (16), as follows:

$$\phi_w = \frac{c_{fw} \cdot u_{max}^2}{2.g.\Delta.D_{50}} \tag{19}$$

The model tests show, see Fig. 18, using the method of linear regression, that:

$$n = 7.2 \cdot 10^7 \, \phi_w^{6.86} \tag{20}$$

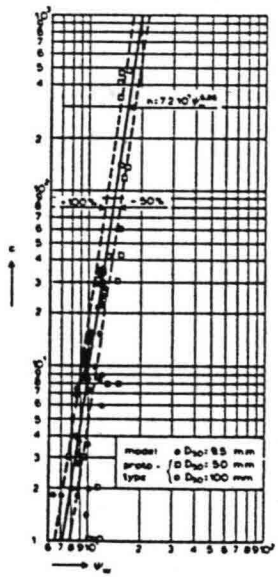

Fig. 18: Transport related to the flow parameter $\phi_w$

From Fig. 18 it can be seen that Equation (20) gives a good prediction of the measured transport in the prototype.

49. If a push tow unit is sailing some distance from the bank, the transport predicted with Equation (20) is overestimated. In these cases a second method is recommended which has been extensively described in ref. 6. This method is more complicated and has been based on the calculation of the shear stress distribution occurring under the stern wave. Using the transport relation of Paintal (ref. 21) and assuming a constant effective transport width, $B_e$, the total transport can be determined by integration over the stern wave length, L:

$$n = \frac{6}{\pi} \cdot c_v^2 \cdot \frac{1}{V_s} \sqrt{\frac{g.\Delta}{D_{50}^3}} \, B_e \int_0^L \phi \, dx \tag{21}$$

50. In practice Equation (21) cannot be applied easily and it has been simplified therefore by using the integral value of $\int_0^L \phi \, dx = \phi_{max} \cdot L_e$ with $\phi_{max}$ representing the maximum

transport parameter and $L_e$ the effective transport length depending on the length L. The important parameters have been computed as follows:

$$\phi_{max} = 13\ \psi_{max}^{2.5} \quad \text{(Paintal)} \tag{22}$$

$$\phi_{max} = \frac{\alpha_z}{2} \cdot \frac{\hat{\Delta h}}{\Delta . D_{50}} \cdot i_{max} \quad (i_{max}\text{: see Equation (5)}) \tag{23}$$

$$\alpha_z = 1 - \frac{2V_s^2}{g.\hat{\Delta h}} \left(\frac{\Delta . D_{50}}{\hat{\Delta h}}\right)^2 \quad (0 < \alpha_z < 1) \tag{24}$$

The following expressions were derived, from the transports measured in the model, to determine $B_e$ and $L_e$:

$$B_e = 1.8\ \hat{\Delta h} \text{ and } B_e L_e = 0.23\ z_o^2 \text{ (see also Equation (6))} \tag{25}$$

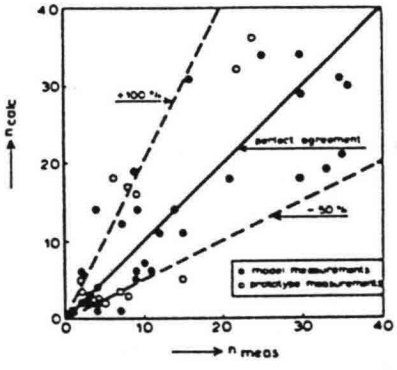


Fig. 19: Computed transport versus measured transport

The data from the prototype experiments, see Fig. 19, show that the method presented gives good results.

51. A formula has been derived, by measuring the lowest level of transport below the undisturbed water level. With this formula it is possible to determine the lowest level of the upper part of the protection construction, see Fig. 3. This formula has the following form:

$$\frac{y'}{D_{50}} = 4.4 \left(\frac{\hat{\Delta h}}{\Delta . D_{50}} - 1.2\right) \tag{26}$$

The applicability of this formula, in practice, is determined by the requirement that the lower part of the protection construction which is subject to the attack of return currents, see Fig. 3, must be stable against the stern wave attack. So, if the $D_{50}$ of the protection material on the lower part and $\hat{\Delta h}$ , the maximum water level depression caused by the stern wave, are known, the lowest level, y', of the upper part below the undisturbed water level can be computed.

52. Secondary waves. A start has now been made to investigate the stability and transport related to ship-induced secondary waves, see ref. 7.. There is considerable information in literature about the stability of rip rap against the attack of waves perpendicular to the slope. In this context use has been made of the Hudson Formula (ref.22):

$$\frac{H}{\Delta . D_{50}} < (K_{RR} \cdot \cot g\alpha)^{1/3} \cdot S_f^{1/3} \tag{27}$$

A value of 2.2 is given for $K_{RR}$ in circumstances of breaking

waves with heigths less then 1.5 m. Assuming the value of $K_{RR}$, valid for the secondary waves, Equation (27) indicates that stability in the prototype and model (cotg$\alpha$ = 4, $S_f$ = 0.65) is guaranteed if $H/\Delta.D_{50} < 1.8$ . However in the tests, see Fig. 20, it was found that no material was transported for values of:

$$\frac{H}{\Delta\ D_{50}} < 3.0 \qquad (28)$$

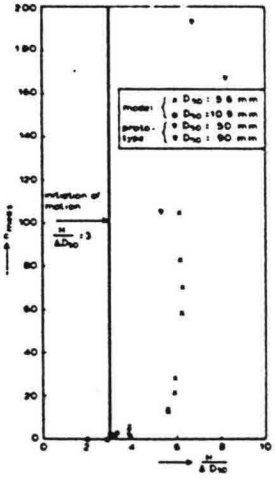

Fig. 20: Transport versus secondary wave parameter

53. The difference between prediction and experiment may be due to several factors including the influence of wave length, $L_w$, on the stability or the different wave propagation direction. In this respect use has been made of the work of Pilarczyk (ref. 23), in which the following stability criterion for perpendicular wave attack was presented:

$$\frac{H}{\Delta.D_{50}} < N_s \cdot S_f^{1/3} \qquad (29)$$

$$\text{with: } N_s = 0.54\ k_E \left(\frac{H}{L_w}\right)^{-0.25}, \text{ (for } \frac{H}{L_w} < 0.05\ \text{tg}\alpha) \qquad (30)$$

$$N_s = 2.25\ (\text{cotg}\alpha)^{0.5}\ k_E \left(\frac{H}{L_w}\right)^{0.25}, \text{ (for } \frac{H}{L_w} > 0.05\ \text{tg}\alpha) \qquad (31)$$

$$k_E = \text{tg}\varepsilon \cdot \cos\alpha + \sin\alpha \qquad (32)$$

In Equation (32) $\varepsilon$ is the natural angle of repose and can be taken at 45° for natural quarry stones, see ref. 23. From the tests it was observed that, in the critical situation - characterized by $H/\Delta.D_{50}$ = 3 in Fig. 20 and Equation (28) - $H/L_w$ had a value of 0.08. This means, with cotg$\alpha$ = 4, that $N_s.S_f^{1/3}$ = 2.5, which is less than the value of 3.0 given in Equation (28).

54. It can be assumed that this small difference is due to the direction of wave propagation, $\Theta$ = 54° . It is recommended that in such cases the wave height should be reduced to $H.(\cos\Theta)^{0.5}$ . Substitution of this reduced value of H in Equation (29) gives:

$$\frac{H}{\Delta.D_{50}} < N_s \cdot S_f \cdot (\cos\Theta)^{-0.5} \qquad (33)$$

In the critical situation mentioned above the stability value for $H/\Delta.D_{50}$ will now increase to 3.3, which is in good agreement with the experimental value, see Equation (28).

55. As in the case of the stern wave an expression to determine the lowest level of the protection zone against the secondary waves, below the undisturbed water surface, has been derived from the measured transport, see Fig. 21:

$$\frac{y'}{D_{50}} = 3.0 \left(\frac{H}{\Delta . D_{50}} - 1.5\right) \qquad (34)$$

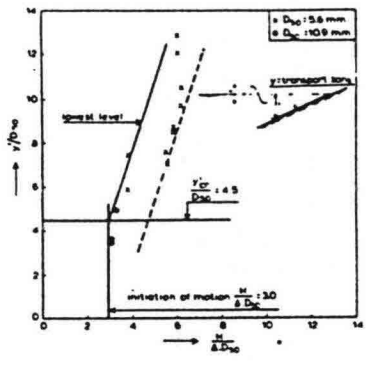

Fig. 21: Lowest level of transport by secondary waves

The applicability of Equation (34) is determined by the requirement that no damage may occur in the lower protection zone, see Equation (26).

56. The upper boundary of the protection zone with respect to the undisturbed water surface, can be determined with the wave run-up formula

$$\frac{R_u}{H} = 2\, c_s \left(\frac{H}{L_w}\right)^{-0.5} \operatorname{tg}\alpha = 2\, c_s\, \xi \text{ (for } \xi < 3) \qquad (35)$$

with $R_u$ = wave run-up and $c_s$ = 0.6 for rip rap

57. Screw race. Stability of bottom and bank protection against the screw race attack is important when ships are manoeuvring near locks and berths.

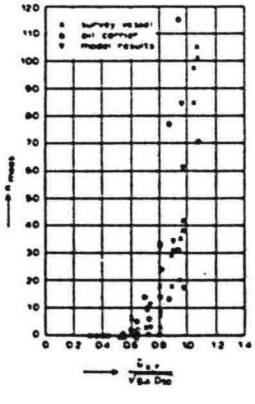

Fig. 22: Transport caused by screw race

For these situations model and prototype experiments indicate that:

$$\frac{u_{x,r}}{(g.\Delta.D_{50})^{0.5}} < c \qquad (36)$$

in which $u_{x,r}$ represents screw-induced current velocities computed with Equation (10) and c is a constant. From Fig. 22 it can be seen that, according to the experiments (ref. 10): c = 0.55 (no transport); c = 0.70 (small transport).

58. The area in which the transport occurs is characterized by, see ref. 10,: $0.05 < z_s/x_s < 0.35$ and $-0.2 < y_s/x_s < 0.2$, in which $x_s$, $y_s$ and $z_s$ are ordinates with the origin in the centre of the screw.

Experimental model for the stability of block revetments

59. A slope revetment consisting of loose blocks derives its strength from the mass of each individual block. Friction between individual blocks increases the strength of the slope revetment. Other factors also may contribute to the strength of a slope revetment, for example, interlocking between blocks, clenching of the blocks, etc. A slope revetment may also derive its strength from the sublayer. In the case of an impermeable sublayer, for example, "good" clay, the pressure

underneath the blocks cannot build-up as easily as in the case of permeable sublayer and this results in a higher revetment strength. However, when erosion of the clay occurs, for example, "poor" clay, the strength of the slope revetment is reduced. In this case, therefore, the strength of the clay, that is, resistance against erosion, is the weakest link.

60. For wave attack (wind waves or ship waves) the downsurge stage is mostly decisive for the possible lifting-up of blocks, that is, the combination of pressure due to the high level of phreatic line and pressure due to the oncoming wave front. A simplistic equilibrium analysis of the stability of blocks placed on a permeable sublayer leads to the following strength equation:

$$\frac{H}{\Delta . D_b} = \frac{\cos\alpha}{K} \qquad (37)$$

where K is an empirical constant (or function) depending on revetment type (friction/interlock between blocks and porosity of revetment) and cooperation with blocks lying above.

61. In the case of ship-induced loads, for example, transversal stern wave and/or secondary waves, the value of K can be roughly taken equal to 0.20 for free blocks and 0.15 for grouted revetments. However, in the latter case, the stability of the filter and/or sublayer may be more critical. The absolute height of a block must not be less than about 0.10 m for it to retain its stability. More exact relationships on the aspects will probably be available when the recent prototype data have been compiled and evaluated.

62. The upper boundary of a block revetment with respect to the undisturbed water surface is directly related to the wave run-up, wich can be computed with Equation (35) taking into account a value of 1.0 for the constant $c_s$.

Mathematical model for the stability of block revetments

63. A mathematical model has been developed by the DSML for the calculation of pore pressures in the layer underneath a block revetment, ref. 15 and 24. The model is based on the solution of the equation for groundwater flow in the layer underneath the blocks, with leach terms to include the seepage through the revetment. The variation of the phreatic line within the filter layer is included by a simultaneous solution of the mass balance equation for the flow to and from the phreatic surface. By using a finite difference code a realistic representation of the revetment as an alternation of blocks and joints is possible. The permeability may be a function of the local hydraulic gradient, thus allowing for turbulent or semi-turbulent flow. Formulae for flow in narrow joints have been derived from special permeability tests. The geometry of the protection may be rather arbitrary in the model; a succession of different slopes is possible. The hydraulic boundary conditions may also be arbitrary, for

example, it is possible to use a tape with measured wave pressures as input for the programme. The programme calculates both pore pressures and the phreatic level as a function of time and place. The following conclusions can be derived from the calculation study: a. The risk of damage to the surface layer decreases with: more permeable revetments and with less permeable or thinner (or even completely absent) underlying (filter) layers; b. The elevation of the mean level of the phreatic surface above its original level increases the more permeable the revetment; however, the pore pressures are then smaller; c. An important parameter for the determination of the quasi-static pressures underneath the revetment is the leach length, defined as $\lambda = \sin\alpha \sqrt{bdk/k'}$, where $\alpha$ is the slope of the dam, b is the thickness of the (filter) layer underneath the revetment, d is the thickness of the revetment and k' and k are the permeability of the revetment and of the filter layer respectively.

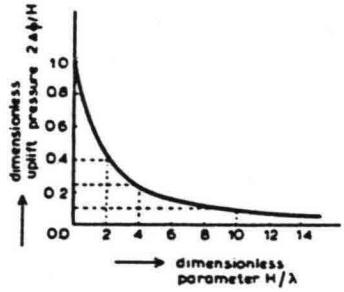


Fig. 23 Uplift pressure under revetment

A pressure-difference curve is given in Fig. 23 based on a horizontal free water surface, which varies sinusoidally in time, with amplitude H.

RECOMMENDATIONS

64. The design rules, presented in this paper, concern the subsoil, the filter layers, the bottom and bank protection constructions of fairways. As input the predicted values of the water motion near the banks and bottom are needed. Until now both the prediction of the water motion and the developed design rules are mainly based on results of measurements with pushing units. To give wider applicability to the design rules presented it is recommended to: (a) make a verification for more varied circumstances as different ship types, channel cross-sections, subsoils; (b) take the influence of more ships at a cross profile into account as well as a verification of the effect of natural currents; (c) elaborate and adapt the formulas given for speed prediction; (d) study the long term effects on the behaviour of the protections and subsoil; (e) check and possibly improve the relations to determine the dimensions of block revetment; (f) develop critical values for internal hydraulic gradients; (g) develop a 3-dimensional model to calculate the ship induced water motion, especially near to the bottom and banks.

ACKNOWLEDGEMENTS

65. The authors like to thank Rijkswaterstaat (Dutch Public Works Department) for their permission to publish results of research carried out at the Delft Hydraulics Laboratory and the Delft Soil Mechanics Laboratory. Also the authors wish to thank mr. H.J. Verhey and mr. M. van der Wal for their support.

NOTATION

| | | |
|---|---|---|
| $B_e$ | effective transport width | m |
| $b$ | waterline width of channel | m |
| $c_{fc}, c_{fr}, c_{fw}$ | shear stress coefficients | - |
| $c_s$ | porosity coefficient | - |
| $c(y)$ | front wave coefficient | $m^{-1}$ |
| $c_v$ | shape parameter | - |
| $D_b$ | block height | m |
| $D_n$ | nominal diameter | m |
| $D_o$ | effective outflow diameter | m |
| $D_p$ | propeller diameter | m |
| $D_{50}, d_{90}$ | characteristic diameters of graded material | m |
| $g$ | gravitation acceleration | $ms^{-2}$ |
| $H$ | wave height | m |
| $H_i$ | height of interference peak | m |
| $h$ | water depth | m |
| $\overline{\Delta h}$ | average waterlevel depression | m |
| $\hat{\Delta h}$ | transversal stern wave height | m |
| $\Delta h_f$ | front wave height | m |
| $i_f$ | front wave steepness | i |
| $i_{max}$ | maximum stern wave steepness | - |
| $i_x, i_y, i_z$ | hydraulic gradients | - |
| $K_{RR}$ | stability factor | - |
| $K_{TP}$ | thrust coefficient of propeller | - |
| $k_D, k_E$ | coefficients | - |
| $k_s$ | roughness | m |
| $L$ | stern wave length | m |
| $L_e$ | effective transport length | m |
| $L_{OA}$ | length overall | m |
| $L_{wi}$ | length of interference peak | m |
| $N_s$ | stability coefficient | - |
| $n$ | number of transported stones | - |
| $n_p$ | number of revolutions | - |
| $O_{95}$ | characteristic open area in geotextile | m |
| $P_S$ | installed engine power | W |
| $R_T$ | total resistance | N |
| $R_u$ | wave run-up | m |
| $r$ | radial distance to screw centre | m |
| $S$ | distance to ship's side | m |
| $S_f$ | shape factor | - |
| $u_c$ | current velocity | $ms^{-1}$ |
| $u_{max}$ | maximum current velocity in transversal stern wave | $ms^{-1}$ |
| $u_r$ | average return current velocity | $ms^{-1}$ |
| $\hat{u}_r$ | maximum return current velocity | $ms^{-1}$ |
| $u_{x,r}$ | screw-induced current velocities | $ms^{-1}$ |
| $u_o$ | outflow velocity | $ms^{-1}$ |
| $V_S$ | ship's speed | $ms^{-1}$ |
| $X$ | distance from ship's bow | m |
| $x_s$ | distance from screw centre | m |
| $y$ | eccentric distance from canal axis | m |
| $y'$ | lowest level of transport | m |
| $z_o$ | stern wave coefficient | m |
| $\alpha$ | slope angle | degrees |
| $\alpha_i$ | coefficient for interference peaks | - |
| $\alpha^z$ | coefficient for transversal stern wave | - |
| $\Delta$ | relative density | - |
| $\eta_D$ | efficiency | - |
| $\varepsilon$ | natural angle of repose | degrees |
| $\Theta$ | angle of wave propagation | degrees |
| $\tau, \hat{\tau}$ | shear stresses | $Nm^{-2}$ |
| $\phi, \phi$ | transport parameters | - |
| $\phi, \phi_w^{max}$ | shear stress parameters | - |

REFERENCES

1. KAA E.J. VAN DE Power and speed of push tows in canals. DHL Publication, No. 216, August 1979
2. BLAAUW H.G. and KNAAP F.C.M. VAN DER Prediction of squat of ships sailing in restricted water. DHL Publication, No. 302, April 1983
3. BLAAUW H.G. and KNAAP F.C.M. VAN DER Prediction of water level depression and squat of ships sailing in restricted water (in Dutch). Report on model investigations, M1115-Part VA, September 1983
4. KAA E.J. VAN DE Hydraulic attack of bank protections (in Dutch). Kust en Oeverwerken, in praktijk en theorie, March 1979
5. WAL M. VAN DER Bottom and bank erosion by the ship induced return current (in Dutch). Report on model investigations, M1115-Part XB, to be published in 1984
6. KNAAP F.C.M. VAN DER Attack of transversal stern wave on rip rap bank revetments (in Dutch). Report on model investigations, M1115-Part XC, April 1982
7. VERHEY H.J. Attack of secondary ship waves on rip rap bank revetments (in Dutch). Report on model investigations, M1115-Part VI, to be published in 1984
8. GATES E.T. and HERBICH J.B. Mathematical model to predict the behaviour of deep-draft vessels in restricted waterways. Texas, A and M University, Sea Grant College, Report TAMU-SG-77-206, 1977
9. BLAAUW H.G. and KAA E.J. VAN DE Erosion of bottom and sloping banks caused by the screw-race of manoeuvring ships. DHL Publication, No. 202, july 1978
10. VERHEY H.J. The stability of bottom and banks subjected to the velocities in the propeller jet behind ships. DHL Publication, No. 303, April 1983
11. PILARCZYK K.W. Prototype tests of slope protection systems. Conference on flexible armoured revetments incorporating geotextiles, London 29-30 March 1984.
12. OLDENZIEL D.M. and BRINK W.E. Influence of suction and blowing on entrainment of sand particles. J. Hydraulics Division, July 1974, 935-948
13. GROOT M.T. DE THABET R. and KENTER, C.J. Soil mechanical design aspects of bank protections (in Dutch). KIVI-Symposium, Delft, 25 May 1983
14. GROOT M.T. DE and SELLMEYER J.B. Wave induced pore pressures in a two layer system. DSML-mededelingen, Delft, Part 2-4, 1979, 67-78
15. SELLMEYER J.B. Uplift pressures under a block revetment (in Dutch), Internal report DSML, Delft, CO-255780, August 1981
16. GRAAUW A. DE MEULEN T. VAN DER and DOES DE BYE M. VAN DER Design criteria for granular filters, DHL-publication 287, January 1983
17. VELDHUYZEN VAN ZANTEN R. Geotextiles in coast- and bank protections (in Dutch) Publication Dutch Association of Coast and Bank protections, Rotterdam, 1982
18. IZBASH S.V. and KHALDRE K.Y. Hydraulics of river channel closure, Butterworths, London, 1970
19. SHIELDS A. Anwendung der Aehnlichkeits-Mechanik und der Turbulentzforschung auf die Geschiebebewegung. Preussische Versuchsanstalt für Wassserbau und Schiffbau, Berlin, 1936
20. NAHEER E. The damping of solitary waves. Journal of Hydraulics Research, Vol. 16, no. 3, 1973
21. PAINTAL A.S. Concept of critical shear stress in loose boundary open channels. Journal of Hydraulics Research, Vol. 9, no. 1, 1971
22. HUDSON R.Y. Design of quarry stone cover layers for rubble mound breakwaters. Waterways Experimental Station (WES), Research report No. 2-2, july 1958
23. PILARCZYK K.W. and BOER K. DEN Stability and profile development of coarse materials and their application in coastal engineering DHL Publication, No. 293, January 1983.
24. BEZUYEN A. STEENZET, a model for calculating uplift pressures under block revetment (in Dutch). DSML, Delft, Internal report CO-258901/91, 1983.

# DUTCH PROTOTYPE EXPERIMENTS WITH BANK PROTECTION SYSTEMS

Appendix 3

Impression of damage to the
test embankments at the Houtrib-dike

Picture 1 : V.O.B.-mat; impression of the deformation of the slope. On the foreground, the transition to the ASAM-mat

Picture 2 : V.O.B.-mat; detail of the slope deformation

Picture 3 : V.O.B./ASAM; transition between both mat types

Picture 4 : ASAM-mat; detail of damage

Picture 5 : ASAM-mat; part of the bank protection slided down along the slope. On the foreground, the transition to the Armorflex section

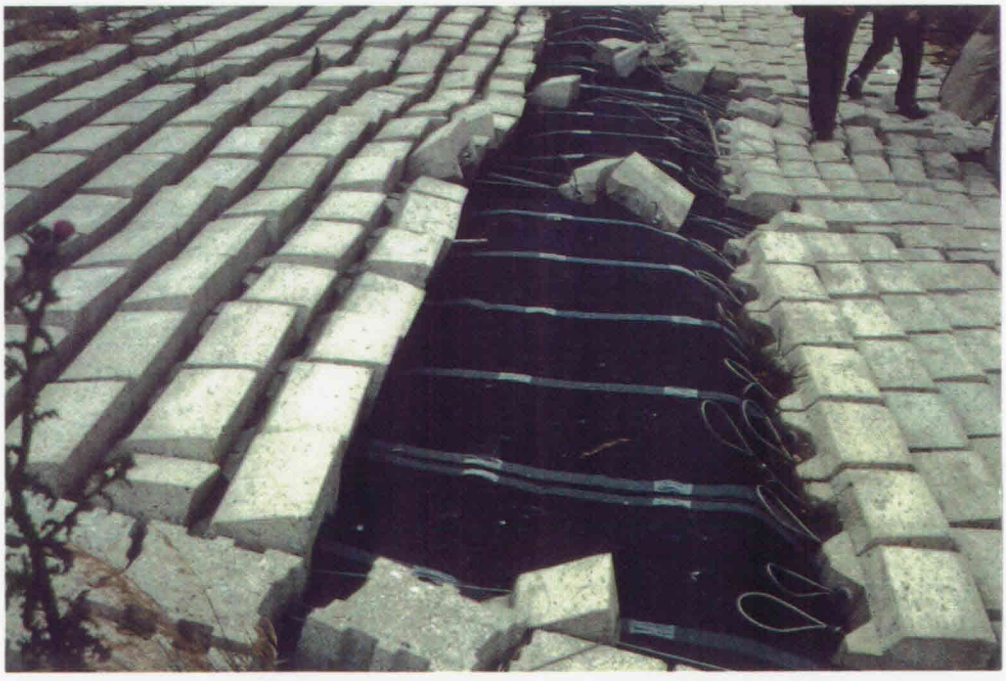

Picture 6 : ASAM-mat; detail of the internal joint between standard mat sections

Picture 7 : Armorflex-mat; detail of damage close to the transition to the Beto-mat

Picture 8 : Beto-mat; impression of the deformation of the slope. On the foreground the transition to the rip-rap reference section

Picture 9 : Beto-mat; detail of damage

Picture 10: Beto-mat; detail of the internal joint between standard mat sections

Picture 11: Beto-mat; over all picture of slope deformation and damage

Picture 12: Beto-mat: part of mat slided down and pushed up against lower mat sections (detail of picture 11)